UNIVERSITY OF SOUTHAMPTON

FACULTY OF PHYSICAL SCIENCES AND ENGINEERING
Electronics and Computer Science

Towards Non-Steady State Rating of Offshore Wind Farm Cables

by

Siew Peng Phuan

Thesis submitted for the degree of Master of Philosophy

November 2015

UNIVERSITY OF SOUTHAMPTON

ABSTRACT

FACULTY OF PHYSICAL SCIENCES AND ENGINEERING
ELECTRONICS AND COMPUTER SCIENCE

Master of Philosophy

TOWARDS NON-STEADY STATE RATING OF OFFSHORE WIND FARM CABLES

Siew Peng Phuan

Wind power plays a significant role in energy production. The future developments of wind power installations are more likely to take place offshore due to space availability, fewer problems with local population acceptance, and more reliable winds. For offshore wind farms, fluctuations in generation can be large as conditions are changeable. There are no specific load patterns to enable the wind farm export cable rating to be calculated based on actual cyclic loads. The existing rule for calculating the rating is based on maximum steady state wind power output which can lead to cable oversizing.

This project focusses on developing non-steady state rating techniques for High Voltage Alternating Current (HVAC) wind farm export cables that apply cyclic rating methods to analyse the effect of different flat-top cyclic load cycles on the thermal performance of a three-core HVAC 132kV XLPE cable. Three FEA cable models are used for testing buried at sea, landfall and J-tube in air cable sections. Sensitivity analysis simplifies the models to minimise computation time required. Five cyclic load profiles are run for each cable section (3 daily and 2 extended cycles above 24 hour).

Results are compared to one year of normalised wind power data from the Cullerin Range wind farm to establish exceedance of the cable temperature limit for each cyclic load. The cycle with the closest fit within limitations is then used to estimate the potential for increasing cable rating.

Contents

List of Figures

List of Tables

Symbols and Abbreviations

Wc	Conductor Joule losses per unit length	$W{\cdot}m^{-1}$
Wd	Dielectric losses per unit length	$W{\cdot}m^{-1}$
Rac	AC resistance of the cable conductor	Ωm^{-1}
Ws	Sheath losses per unit length	$W{\cdot}m^{-1}$
Cd	Capacitance of dielectric	F
Uo	Applied voltage between conductor and sheath	V
T	Temperature	°C
tanδ	Dielectric loss factor	
I	Cable current rating	Ampere
n	Number of conductors in a cable	
q	Heat flux due to dielectric losses	Wm^{-2}
f	Frequency of applied voltage	Hz
hc	Heat transfer coefficient for convection	$Wm^{-2}K^{-1}$
c	Distance between cable axis and conductor axis	m
d_B	Average diameter of the armouring layer	m
R'_B	Resistance per meter of the armouring	Ωm^{-1}
R'	Resistance per meter of the conductor	Ωm^{-1}
R'_S	Resistance per meter of the lead sheath	Ωm^{-1}
s	Axial distance of the conductors	m
d	Average sheath diameter	m
t_1	Thickness between conductor and sheath	mm

ρT	Thermal resistivity of the insulation material	KmW^{-1}
t_2	Thickness of the bedding	mm
Ds	Outer diameter of the sheath	mm
t_3	Thickness of the serving/outer sheath	mm
D′a	Outer diameter of the armouring	mm
$\Delta\theta$	Conductor temperature rise above ambient	°C
T_1	Thermal resistance between conductor and sheath per unit length	KmW^{-1}
T_2	Thermal resistance of the bedding between sheath and armour per unit length	KmW^{-1}
T_3	Thermal resistance of the serving per unit length	KmW^{-1}
T_4	Thermal resistance between cable surface and the surrounding medium	KmW^{-1}
λ_1	Ratio of losses in the metal sheath to total conductor loss	
λ_2	Ratio of losses in the armour to total conductor loss	
ρT	Thermal resistivity of soil	KmW^{-1}
D_e	Outer cable diameter	mm
L	Burial depth/vertical distance between the seafloor	m
T_c	Conductor temperature	°C
M	Cyclic overload rating factor	
μ	Loss-load factor	
k	Ratio of cable external surface temperature rise above ambient to conductor temperature rise above ambient under steady conditions	
$\beta(t)$	Attainment factor for cable surface	
Ei(x)	Exponential integral function.	
Q'_{rad_ext}	Radiation losses from J-tube	Wm^{-1}

A_{OR}	Lateral area of the J-tube	m^2
θ_{OR}	Outside Temperature of J-tube	K
θ_{surf}	Ambient Temperature around the J-tube	K
σ	Stefan-Boltzmann Constant	$Wm^{-2}K^{-4}$
ε_R	Emissivity of the outside surface of the J-tube	
h_{int}	Heat transfer coefficient of the cable surface	$Wm^{-2}K^{-1}$
θ_{cable}	Temperature of the cable surface	K
θ_{tube}	Temperature of inner J-tube surface	K
L_{tube}	Length of the tube	m
g	Gravity	ms^{-2}
β	Coefficient of volumetric expansion	1/K
θ_J	Temperature of cable surface	K
θ_{IR}	Temperature of the inside of the riser	K
Pr	Dimensionless Prandtl number	
υ	Kinematic viscosity	m^2s^{-1}
c and n	Constants required to determine the Nusselt number	
h_{ext}	Heat transfer coefficient of the J-tube surface	$Wm^{-2}K^{-1}$
θ_{ambient}	Temperature of the ambient temperature	K
α	Absorptivity of the J-tube	
Qsolar	Solar heat flux	

Declaration of Authorship

I, **SIEW PENG PHUAN** declare that this thesis and the work presented in it are my own and has been generated by me as the result of my own original research.

TOWARDS NON-STEADY STATE RATING OF OFFSHORE WIND FARM CABLES

I confirm that:

1. This work was done wholly or mainly while in candidature for a research degree at this University;

2. Where any part of this thesis has previously been submitted for a degree or any other qualification at this University or any other institution, this has been clearly stated;

3. Where I have consulted the published work of others, this is always clearly attributed;

4. Where I have quoted from the work of others, the source is always given. With the exception of such quotations, this thesis is entirely my own work;

5. I have acknowledged all main sources of help;

6. Where the thesis is based on work done by myself jointly with others, I have made clear exactly what was done by others and what I have contributed myself;

7. Either none of this work has been published before submission, or parts of this work have been published as: N/A

Signed: ……

Date: ……

Acknowledgements

I would like to extend my deepest gratitude to the following who have encouraged, inspired, supported and assisted in my pursuit of this Master of Philosophy degree.

First and foremost, I would like to thank University of Southampton for offering this MPhil/PhD course and the studentship. Without it, I would not have be able to pursue my study. I would like to also thank my supervisor, Professor Paul L. Lewin for his advice and support in continue with this research study.

Secondly, I would like to offer my sincere thanks to my second supervisor, Dr. James A. Pilgrim who has guided me throughout my thesis with his patience, knowledge and support.

Thirdly, I would like to thank Dr. Richard Chippendale for his help, tuition and guidance for the modelling work in this thesis.

Finally, I thank my husband Andy Swindell and my mum Mui-Lay Teo for supporting me emotionally throughout my studies.

Without the support, encouragement, and dedication to assist me, this thesis would not have been possible.

Chapter 1

Introduction

Renewable energy plays an increasing role in the supply of energy worldwide. Wind energy production has substantially increased over recent years, a trend that looks set to continue as global energy demand increases, and nations look to break their dependence on non-renewable energy sources. According to the calculation released by Global Wind Energy Council (GWEC) [1], it shows that wind energy could reduce up to 65% of the emissions that are pledged by industrialized nations.

European Union (EU) states that the future developments of wind power installations are more likely to take place offshore due to space availability, less problems with local population acceptance, and more reliable winds [2]. One of largest leading UK energy companies, E.ON, states that offshore wind farms operate at full power up to 45% of the time [3].

Wind Farm export cables represents one of the capital expenditure for the construction of offshore wind farms. In order for the design of the wind farm export systems to be efficient and reduce the cost of energy associated with offshore wind farms, the size of the cables need to be rated accurately. Subsea cables need to transmit power to shore with sufficient current carrying capacity that the conductor temperature does not exceed its permissible threshold limits.

The highly fluctuating power output generated by wind farms increases the level of difficulty in calculating the subsea cable rating more accurately. With the traditional calculation rules, based on thermal models with steady state conditions and maximum load, this approach often leads to cables being oversized compared to actual requirements. Incorrectly rated subsea cable can lead to poor asset utilisation.

1.1 Research Objective

The most common and traditional calculation method used to ensure that the conductor temperature remains within the threshold of the insulating material is IEC60287 [4]. For the

subsea cables, the most commonly used insulating material is cross-linked polyethylene (XLPE), which typically has a thermal limit of 90°C.

IEC 60287 [4] is based on the thermal network approach to represent the heat generation and dissipation in a cable. This method is simple but contains a lot of inherent assumptions and simplifications. The primary purpose is to provide a steady state rating which ensures that the conductor temperature does not exceed the limits that would consequently cause degradation to the cable.

New modelling techniques are essential to reduce the cost of connecting offshore renewable energy projects to the grid. Using non-steady state rating modelling to assess cable requirements more accurately, would result in smaller cables, a reduction in connection cost, without a reduction in reliability. This project focusses on developing non-steady state rating techniques for wind farm export cables applicable to existing alternating current (AC) transmission systems.

Figure 1.1 shows an overview of a whole installation from the land to the wind turbine. The thermal sections of the cable considered for this project are (1) burial at sea, (2) J-Tube and (3) Landfall section.

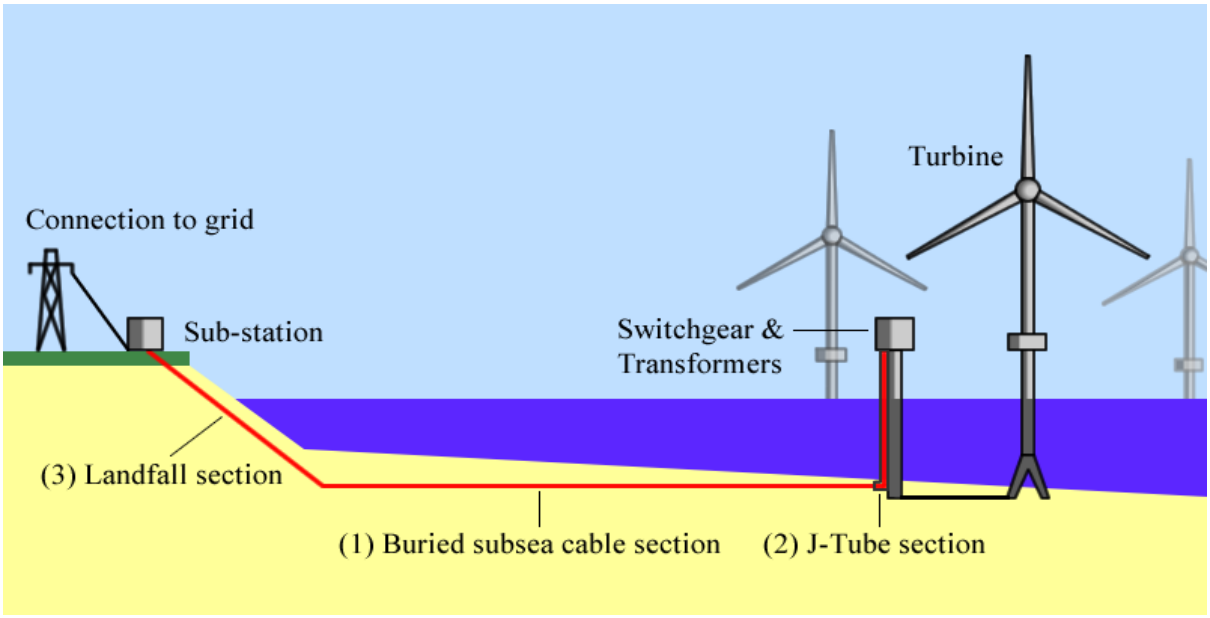

Figure 1.1: Typical Layout of an Offshore Wind Farm [5]

1.2 Research Outcome and Contributions

This research work shows that using cyclic rating methodology on cable sections with long thermal time constants, has the potential for a significant increase in cable rating over steady state method. Comparing actual wind farm output data with a range of test load cycles of differing durations, showed the output as being most closely related to test cycles of relatively short duration. The most significant improvement is seen for the landfall section, a thermal pinch point in the export cable system, where a daily cycle of 18 hours high and 6 hours low resulted in a potential increase in cable rating of 15.07% from 630A to 725A without any risk of exceeding the cable's thermal limit.

Comparing load cycles with the output of live data by identifying the risk of cable thermal limit exceedance, offers a new and relatively straightforward way of quickly assessing the level of cable underutilisation.

The work contributes results that prove cyclic rating methodology is suited for use in offshore wind farm export cable rating. It also acts as a basis for other researchers to further develop and investigate the cyclic rating method and risk factor of cable temperature exceedance with other wind farm datasets.

1.3 Report Organisation

The report consists of six chapters organised in a way to demonstrate the work in developing the non-steady state rating technique for the wind farm export cables.

Chapter 2 presents a literature review of the cable background which contains information on construction, existing steady state and non-steady state cable rating methods, major factors that affect wind farm cable rating, and different sections of the wind farm cable. It also provides an overview of previous research done based on non-steady state rating methods (IEC 60853-2, Finite Element Analysis (FEA) and Probabilistic Rating Technique).

Chapter 3 describes the development of a 2D FEA model for a three-core HVAC 132kV XLPE cable using commercial FEA software Comsol. Sensitivity analysis techniques have been

applied to the following model parameters: armour, conductor and dielectric screen, water tape, sheath screen, binder tape and fillers. The objective of simplifying the model in this way is to minimise the computation time needed to run simulations.

Chapter 4 investigates the application of conventional cyclic rating methods to analyse the effect of different flat-top cyclic load cycles on the thermal performance of the cable model. The development for 3 FEA cable sections running from the land based substation to the offshore windfarm are also presented. The 3 defined cable sections are buried at sea, landfall and J-tube in air sections. Different daily and non-daily cyclic load profiles are applied to all the cable sections for cable thermal behaviour analysis.

Chapter 5 presents analysis of the risk of exceedance for designing the cable system using cyclic methodology. One year of Cullerin Range wind farm power data is applied to the landfall FEA model set in summer season. The load currents are classified into high and low loads to obtain the Probability Density Frequency (PDF) plot of high and low load cycle durations. This is to establish any trends present in the wind farm data that can be compared to the 5 cyclic loads simulated in Chapter 4. Comparison are then used to assess the risk of cable temperature exceedance for these 5 different cyclic load patterns, to see which will be the most suitable base case for an increased cable rating.

Finally, chapter 6 summarises the whole report and possible future work for this research topic.

Chapter 2

Literature Review

For the construction of offshore wind farms, the main components are wind turbines, ground foundations, array cables, electrical offshore substation, high voltage export cables, installations and logistics, and onshore substations. According to E.ON's fact book [3] , the high voltage export cables contribute approximately 5% of capital expenditure of the overall project. The European Wind Energy Association (EWEA) [6, 7] predicts wind capacity investments for offshore wind farms in Europe, will see a rapid increase from approximately €1 billion (year 2010) to €16 billion (year 2030) and will overtake onshore wind farms by 2023 as shown in Figure 2.1 [6, 7]. Based on this potentially huge future investment [6, 7] a better rated, smaller size cable would represent a significant reduction in overall cable construction costs.

Due to the relatively long thermal time constant of cables (especially buried cables), a transient period of 24 hours or even longer is needed for the temperature to reach the equilibrium conditions on which steady state ratings are based.

As the loads in wind farm power cables are cyclic and not sustained, one way of achieving this is to derive a cable rating method based on the variable conditions present in the wind farm environment, where elements such as the electricity generated and the thermal surrounding of the cable, exhibit variations with time.

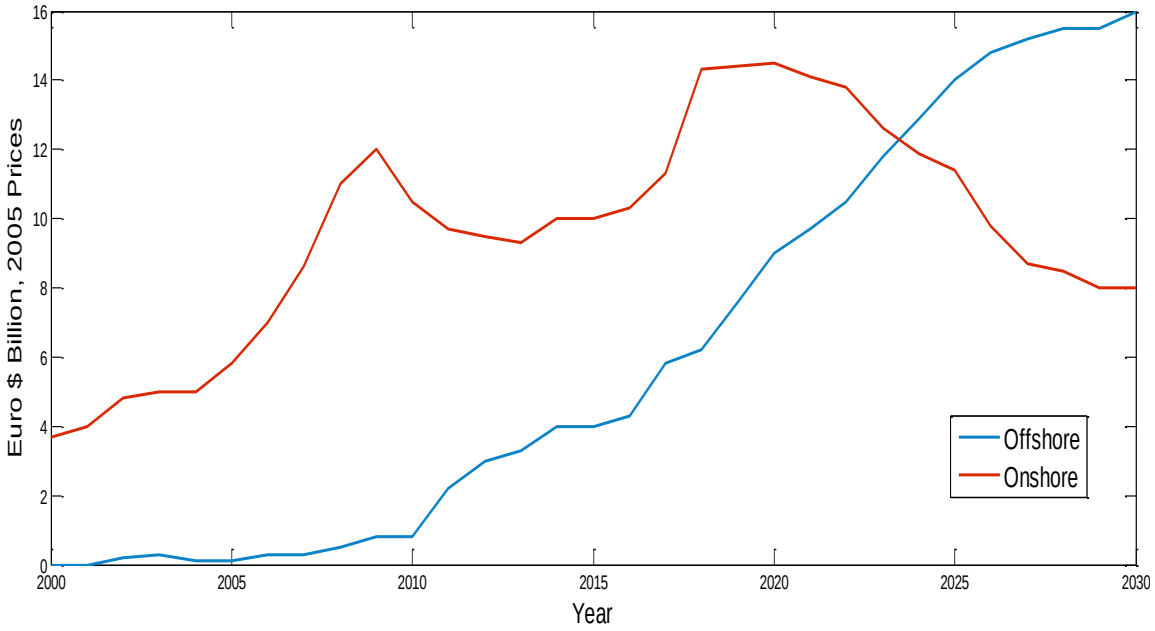

Figure 2.1: Predicted Wind Capacity Investments in Europe [6, 7] Source EWEA (2009).

To better understand all the components needed for achieving the objective, this section provides a detailed literature review on wind farm cable rating methods covering the following aspects: (1) Background of wind farm export cables, (2) Steady State cable rating method, (3) Non Steady-state cable rating methods, and (4) Factors to be considered that influences transient rating method for all sections of wind farm cables (Burial at seabed, Landfall and J-tube).

2.1 Construction of Wind Farm Export Cable

This section examines the construction of typical cables and explains the four main heat losses that occur in cables during operation.

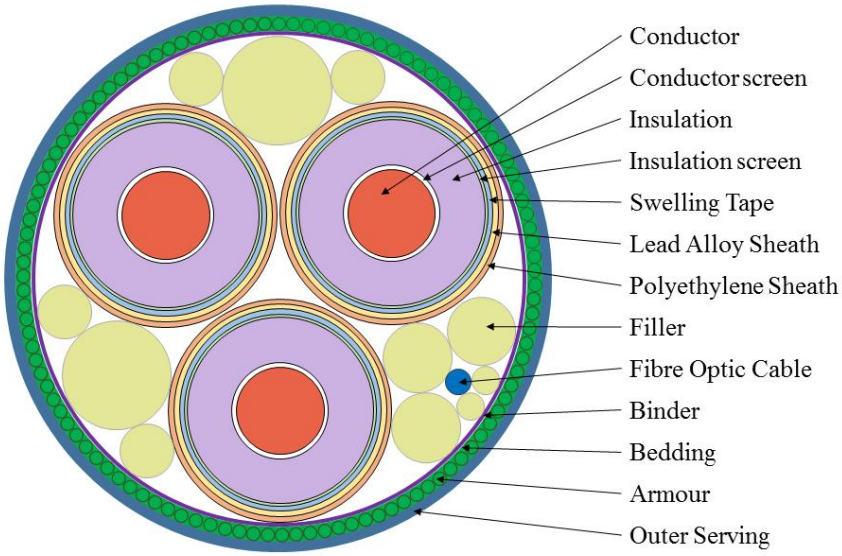

Figure 2.2: Diagram of Three-Core 132kV Wind Farm Export Cable [8]

The construction of the submarine cable is described in detail in this section based on [9]. The conductors which carry the current are made of high-conductivity stranded annealed copper. To maintain a uniform electric field and minimise electrostatic stresses, extruded semi-conducting XLPE is used to screen the conductors. The dielectric system of the cable is made up of three layers and they are conductor screen, conductor insulation and insulation screen. The material for conductor insulation is normally Cross-linked polyethylene XLPE or EPR. XLPE cables have several advantages over Mass Impregnated insulation according to [9] such as lighter in weight, quicker to manufacture, more mechanically robust and operate at higher temperature. However, standard XLPE is not suitable for HVDC applications because of space charge phenomena due to direct current (DC) stress built-up in the insulation [10, 11]. The material for the insulation screen is typically an extruded semi-conducting material and has a similar function as the conductor screen, which is to control the electric field.

Unlike land cables, there is a need to protect against water ingression for submarine cable. The swelling tapes and metallic sheath are used as a water barrier. The material used for sheaths are typically lead alloys, which generally provide better earth fault capacity and water blocking, however, the lead alloy sheathes are used only for export cables and not array cables. Array cables are usually Medium Voltage (MV) of 33kV and are used to link the wind turbines to each other and to the offshore substation. The export cables are usually HV cables of 132kV or

150kV cables and used to transport the electricity brought to the substations by the array cables back to the onshore power grid. An extruded polyethylene jacket is wrapped around each insulated and sheathed conductor to provide an impermeable barrier against water for corrosion protection of the metallic conductor sheath. The submarine cable construction is completed with an overall jacket and then armouring. Finally, the armour is coated with corrosion protection made up of a 50µm zinc layer which is then flushed with hot bitumen during manufacturing. The material for the outer serving (see Figure 2.2) is typically an extruded polymer sheath (such as polyethylene) [9].

2.2 Generators of Heat in Wind Farm Cables

During operation, cables suffer electrical losses which appear as heat in the conductor, insulation and other metallic components. The current rating is dependent on the way this heat is transmitted to the cable surface and then dissipated into the surrounding environment. Cable rating studies usually involve computation of the permissible current flowing in the conductor for a specified maximum operating temperature of the conductor. The current causes the cable to heat, and the limit of loading capacity is determined from the acceptable conductor temperature [4, 13]. Figure 2.3 shows a typical 3-core cable system heat model used for calculating the current rating.

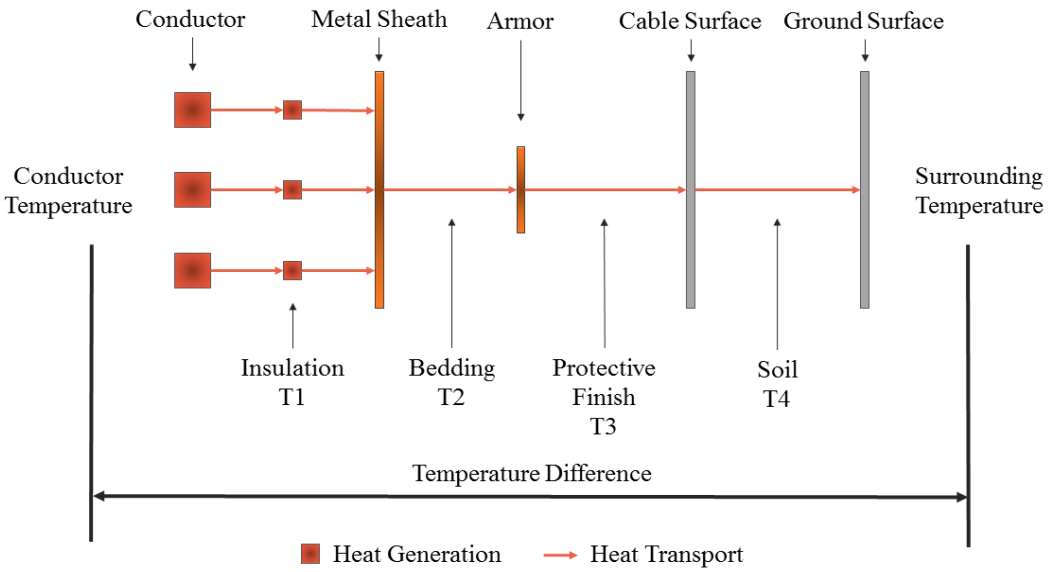

Figure 2.3: Heat Model of Three-Core Cable [12]

There are three main heat sources generated which occur in the (1) conductors, (2) insulation, (3) sheath and armour. These heat losses in a power cable are divided between current dependent and voltage dependant losses [13]. The heat generated is dissipated to the surroundings so the rating of a cable also depends on its immediate environment. A buried cable would have a different rating to one in air due to the different properties of those surroundings to dissipate heat. Each heat source will be then be multiplied by the thermal resistance of each layer it has to pass through (T_1, T_2, T_3, T_4). The thermal resistivity of the four thermal layers T_1 to T_4 are defined according to IEC60287 part 2 [14]

- T_1: Thermal resistance of the dielectric insulation.
- T_2: Thermal resistance between metallic screen/sheath and armouring. (This layer also includes bedding layers under the armouring).
- T_3: Thermal resistance of the outer sheath (serving) over the armouring
- T_4: The accumulated thermal resistance between the buried cable and the sea floor (for buried submarine power cables the heat flow continues through the seafloor soil)

To calculate the cable rating, all the heat losses and thermal resistance will need closer investigation as elaborated in the coming section.

2.2.1 Conductor Losses

All cables will have losses generated by the current flowing in the conductor, originating from the electrical resistance to the current flow in the conductor. It is the most significant loss and are function of both load current and also temperature [4, 13].

$$W_c = I^2 R_{ac} \quad (1)$$

Where W_c is the Joule Loss ((Wm^{-1}), I is the conductor current (A), R_{ac} is the AC resistance of the conductor at maximum operating temperature (Ωm^{-1})

IEC definition of conductor resistance can be found in IEC 60228 [15].

2.2.2 Dielectric Losses

Dielectric loss is voltage dependent and occurs due to the imperfect insulator which causes a leakage current [16]. The insulation of the cable acts as a large capacitor, leading to charging current flows within the insulation when it is subject to AC voltage. When a voltage is applied to the conductor, this will produce a capacitive and a resistive current. The capacitive current is shifted by 90° and the resistive current is in phase with the voltage. This resistive current will generate heat and is considered a loss current. The generated heat results in real power loss which is captured in the loss angle tanδ and is referred to as dielectric loss (W_d) shown in equation (2).

$$W_d = 2\pi f C U_o^2 \tan\delta \quad (2)$$

Where W_d is the dielectric loss per unit length (Wm^{-1}), f is the frequency (Hz), C is the capacitance per unit length (Fm^{-1}), U_o is the voltage to earth (V), tanδ is the loss factor of the insulation at power frequency and operating temperature.

These losses are not uniformly distributed due to the dielectric stress being dependent upon radius, even in a homogeneous insulation according to [12]. Electrostatic stress causes the density of heat generation to be at its highest next to the conductor, and decreases further from it [15]. This phenomena is due to the fact that the electrostatic stress distribution remains constant at all cable operating temperature whereas the permittivity of the dielectric only remains substantially constant throughout the cable operating conditions.

2.2.3 Sheath Losses

Sheath loss is due to the magnetic field associated with the current flow in the conductor which induces electromagnetic fields (EMF) in the sheath of the cable and also in the sheathes of the surrounding cables [15, 17].

$$W_s = \lambda_1 I^2 R_{ac} \quad (3)$$

Where W_s is the sheath loss per unit length (Wm^{-1}), λ_1 is the sheath loss factor, I is the conductor current (A), R_{ac} is the AC resistance of the conductor at maximum operating temperature (Ωm^{-1})

According to [9], there are two types of losses generated in sheaths and screens. They are caused by circulating currents in the sheath λ_1' and eddy currents in the sheath λ_1''. The sheath circulating loss (λ_1') occurs in three-core separate lead sheath (SL type) cables. This is caused by induced currents flowing along the metallic sheath and returning through the sheath of other cable phases or through earth. The sheath eddy loss (λ_1'') is caused by induced eddy currents. The alternating conductor current generates an EMF in the metallic sheath which in turn drives the eddy current inside the metallic sheath. The amplitude of the eddy current is strongly dependent on the thickness of the materials involved and geometric factors. λ_1'' can be ignored as they are negligible compared to λ_1'. λ_1'' can therefore be assumed to be zero for the size of conductors used in three core cables [9].

2.2.4 Armour Losses

In the majority of cases, the armour for the submarine cables is usually multipoint grounded and hence circulating losses are produced therein [9]. Multiple-point grounded means the metallic armour is grounded at the two extreme ends of the cable. If the armour is made of non-magnetic material, the armour and sheath losses are considered together in rating computations. However, the majority of the armoured cables are constructed with magnetic steel wire or tape. According to [18], armour loss equations are probably originated from the measurements performed by ERA [19]. Recent research works [18, 20, 21] have shown that armour losses calculated using the IEC60287 standard are overestimated.

Equation (4) shows calculation for armour loss from IEC60287:

$$\lambda_2 = \lambda_2' + \lambda_2'' = 1.23.\frac{R'_B}{R'}.\left(\frac{2c}{d_B}\right)^2.\frac{1}{1+\left(\frac{2.77R'_B\,10^6}{\omega}\right)^2}.\left(1-\left(\frac{R'_S}{R'}\right)\frac{1}{1+\left(\frac{R'_S}{X'}\right)^2}\right) \quad (4)$$

Where λ_2' is the armour circulating loss, λ_2'' is the armour eddy loss, c is the distance between cable axis and conductor axis (m), d_B is the average diameter of the armouring layer (m), R'_B is the resistance per metre of the armouring (Ωm^{-1}), R'_S is the resistance per metre of the lead sheath (Ωm^{-1}), R' is the resistance per meter of the conductor (Ωm^{-1}), s is the axial distance of the conductors (m) and d is the average sheath diameter (m).

2.2.5 Thermal Resistance

This section will discuss the thermal resistance factors which are restricting the permissible heat flow over a certain cross section of cable. The calculations of internal (T_1, T_2 and T_3) and external (T_4) thermal resistances of cables laid in free air, ducts and buried, are explained in Part 2 of IEC 60287 [14].

The thermal resistance of the insulation (T_1) is only influenced by the cross section of the conductor and the type and thickness of insulation. As the main property of the insulation is to prevent short circuits in the cable its dimension is determined mainly by the applied voltage and cannot be altered for heat transfer improvement. All thermal resistance equations are taken from IEC 60287 [14]. The equation to calculate T_1 is:

$$T_1 = \frac{\rho_\tau}{2\pi}\ln\left(1+2\frac{t_1}{d_c}\right) \quad (5)$$

Where t_1 is the thickness of insulation that is between conductor and sheath (mm), d_c is the diameter of conductor (mm) and ρ_τ is the thermal resistivity of the insulation material (KmW^{-1})

T_2 represents the thermal resistance in the bedding of the 3 insulated conductor cores and has only a small influence on the rating of the cable (calculated at approximately 2% of T_1). It is calculated similar to T_1 and as given in equation (6).

$$T_2 = \frac{\rho_\tau}{2\pi} \ln\left(1 + 2\frac{t_2}{D_s}\right) \tag{6}$$

Where t_2 is the thickness of the bedding (mm) and D_s is the outer diameter of the sheath (mm) and ρ_τ is the thermal resistivity of the insulation material (KmW^{-1}).

T_3 represents the thermal resistance of the outer covering and has a larger influence on the cable rating than T_2 (calculated at approximately 7-8% of T_1). It is given in equation (7).

$$T_3 = \frac{\rho_\tau}{2\pi} \ln\left(1 + 2\frac{t_3}{D'_a}\right) \tag{7}$$

Where t_3 is the thickness of the serving/outer sheath (mm) and D'_a is the outer diameter of the armouring (mm) and ρ_τ is the thermal resistivity of the insulation material (KmW^{-1}).

T_4 represents the thermal resistance of the soil where the cable is buried. This is the main influence factor together with T_1 on the current rating of the cable. It depends on the outer diameter of the cable, the buried depth and the thermal resistivity of the covering. For single buried cables, T_4 is calculated according to Equation (8) and (9):

$$T_4 = \frac{\rho_\tau}{2\pi} \ln\left(u + \sqrt{u^2 + 1}\right) \tag{8}$$

$$u = \frac{2L}{D_e} \tag{9}$$

Where ρ_τ is the thermal resistivity of soil (KmW^{-1}), D_e is the outer cable diameter (mm) and L (mm) is the burial depth/vertical distance below the seafloor.

2.3 Steady State Rating Method

There are a variety of international cable rating standards which are published by IEC, Cigre and other industry bodies [22]. HVAC wind farm cable ratings are most commonly based on the principles of IEC 60287standards [4, 23].

2.3.1 IEC 60287: Steady State Rating

IEC 60287 [4] is an analytical method for the calculation of the steady state current ratings of buried cables, in ducts or in free air operating at all alternating voltages and direct voltages up to 5 kV. It is based on the thermal analysis method developed by Neher-McGrath [24]. The steady state rating is a method that is based on the maximum constant current which the cable circuit can carry [25]. The standard consists of three parts: Part 1: Formulae for current ratings and power losses, Part 2: Formulae for thermal resistance and Part 3: Sections on operating conditions.

The general current rating equations and operating losses are covered in part 1 of IEC 60287 [4]. It is based on a simple 1D thermal network representation for radial heat transfer within the cable cross section and applies partial differential equations to describe longitudinal heat transfer. The general rating, I, is shown in equation (10) [4].

$$I = \left[\frac{\Delta\theta - \mathrm{W}d[0.5T1 + n(T2 + T3 + T4)]}{RT1 + nR1(1+\lambda1)T2 + nR(1+\lambda1+\lambda2)(T3+T4)}\right]^{0.5} \quad (10)$$

Where $\Delta\theta$ is the conductor temperature rise above ambient (°C), R is the conductor AC resistance at maximum operating temperature per unit length (Ωm^{-1}), W_d is the dielectric loss per unit length (Wm^{-1}), T_1 is the thermal resistance between conductor and sheath per unit length (KmW^{-1}), T_2 is the thermal resistance of the bedding between sheath and armour per unit length (KmW^{-1}), T_3 is the thermal resistance of the serving per unit length (KmW^{-1}), T_4 is the thermal

resistance between the cable surface and the surrounding medium (KmW^{-1}), n is the number of load carrying conductors in the cable, λ_1 is the ratio of losses in the metal sheath to total conductor loss and λ_2 is the ratio of losses in the armour to total conductor loss.

IEC 60287 [14] assumes uniform thermal characteristics for area surrounding the cable and that the ground surface is isothermal. D. Swaffield et al. [26, 27] have shown that with the isothermal ground assumption, the cable is over-rated especially in the shallow buried cables. Recent work done by M.S. Baazzim et al. [28] further proved that IEC are less accurate with shallower cable depth.

Many review papers [20, 21, 23, 29-33] use IEC standards to calculate rating for wind farm export cables. J.J. Bremnes et al. [20] and D. Palmgren et al. [21] have justified the armour loss calculation using IEC60287 and comparing with experimental results. X. Yuan et al. [32] integrated the cable design based on IEC60287 standard into power system load flow design thereby achieving a more controllable result for industry related applications.

2.4 Non-Steady State Rating Methods

With wind farm power output being highly fluctuating and unpredictable, using IEC 60287 to obtain the current rating based on steady state condition is considered too conservative. The non-steady state method to obtain the rating for an export cable is a more realistic way.

Combining the heat loss equations specified in the IEC 60853-2 [34] standard, into the Finite Element Analysis (FEA) cable, is another method of providing a more accurate rating based on transient conditions. FEA modelling techniques have advanced significantly due to modern computing systems. Another non-steady state rating method is probabilistic rating which was investigated due to the random variations of some cable thermal parameters.

2.4.1 IEC 60853: Transient Rating

IEC 60853 Part 2 [34] is an analytical method for the calculations of cyclic and emergency current ratings for cables. The internal thermal capacitance needs to be considered for this method and it is applicable for cables operating at voltages of 36kV or more. Thermal

capacitance is considered negligible for lower voltage cables, hence they are not rated by this method.

The method divides the cable thermal circuits into two independent parts for calculating the temperature response of a cable. The first part is made up of the cable components to the outer surface of the cable, and the second part is the environment in which the cable will be operational. This method assumes that soil thermal resistivity and diffusivity are constant, ground surface is isothermal and same load cycle is used for all kind of cables [34].

The various layers of the power cables and ambient soil are represented with the thermal model made up of thermal resistances and thermal capacitances which can be referred to as Cauer network [9] as showed in figure 2.4. When a load is switched on, a constant conductor loss is generated. The conductor losses heat up the conductor which is represented by thermal capacitance, and the conductor temperature follows a logarithmic curve until a steady-state condition is reached. As the conductor heats up, an increasing temperature difference between the conductor and the ambient causes an increasing heat flux through the insulation which is represented by thermal resistance. The increasing heat loss through the insulation reduces the thermal power available for heating up the conductor, and thus, the steepness of the temperature rise curve decreased. The heat capacitance will have an effect on the time constant. A higher heat capacitance of the material will cause a longer time to heat up.

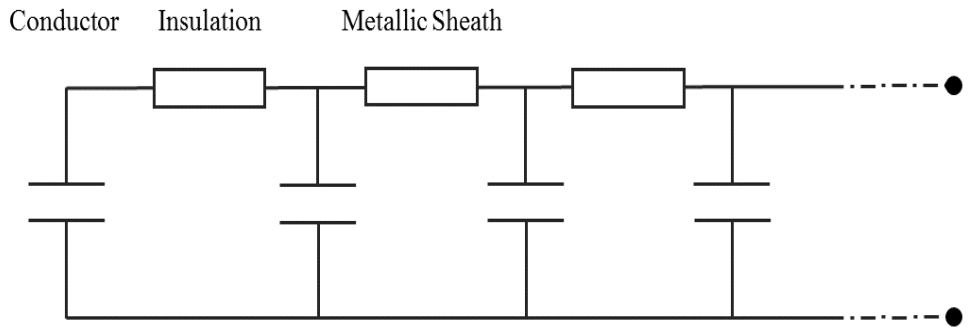

Figure 2.4**:** Cauer Thermal Network [9]

The thermal capacitance of common material types are given in IEC 60853-2 [34], with relevant values for this study presented in Table 2.1.

Table 2.1: Thermal Capacitance

Material	Thermal Capacitance ($J.m^{-3}K^{-1}$)
Paper	2.0×10^6
PE	2.4×10^6
XLPE	2.4×10^6
Copper	3.45×10^6
Lead Alloy	3.8×10^6
Steel	3.8×10^6

The general equation for the thermal capacitance of a given volume V of a material with the specific heat cp is showed in equation (11):

$$C = cp.V.\rho \tag{11}$$

Where C is the Thermal capacitance of material, V is the volume of a material, cp is the specific heat of material, and ρ is the density of material.

2.3.3.1 Cyclic Rating

IEC60853-2 [34] state that the largest current of a cyclic load can be larger than the steady state ampacity. Cables, particularly those buried, will take up to 24 hours or even longer to reach the equilibrium state on which the steady state ratings are based. However, loads are often cyclic rather than sustained and this creates cooling periods between the high load periods [15]. The highest temperature obtained from the cyclic loads can be raised to the maximum permissible cable temperature to obtain the cyclic rating.

The ratio of permissible peak value of current during a daily (24 hour) cycle I_{max} to rated current I_R corresponding to the cable layout conditions is defined as cyclic overloading rating factor.

$$M = \frac{I_{max}}{I_R} \tag{12}$$

Where M is the cyclic overload rating factor, I_{max} is highest permissible rated current during the 24 hour cycle and I_R is the steady state rated current.

This factor is calculated based on the transient thermal analysis of power cables. There are assumptions made in IEC 60853-2 to simplify the analysis. IEC 60853-2 states that for a load cycle of unknown shape but with a known loss-factor (μ), this cycle is considered as a flat top load cycle. A flat-top load cycle as defined by IEC 60853-2 must have a sustained maximum current for a minimum period of 6 hours and the maximum cable temperature rise must occur at the end of the duration of the sustained maximum current. Previous load is considered constant and power losses are represented by using an average loss value during cycle. If the time of the maximum temperature occurs is unknown, the reference time is taken at which the current load was maximal. The electrical resistance of the conductor is considered to be constant and equal to the resistance at the full rated temperature. Under these assumptions, the cyclic loading factor is determined as:

$$M = \frac{1}{\left(\mu\left(1-\frac{\theta_R(6)}{\theta_R(\infty)}\right)+\sum_{t=0}^{5}\left(\frac{\theta_R(t+1)}{\theta_R(\infty)}-\frac{\theta_R(t)}{\theta_R(\infty)}\right)\right)^{\frac{1}{2}}} \tag{13}$$

Where μ is loss-load factor and $\theta_R(t)$ is the conductor temperature rise at above ambient after application of I_R , neglecting variation of conductor resistance.

$$\frac{\theta_R(t)}{\theta_R(\infty)} = \propto (t)(1-k-\beta(t)k) \tag{14}$$

Where k is the ratio of cable external surface temperature rise above ambient to conductor temperature rise above ambient under steady conditions, and $\beta(t)$ is the attainment factor for cable surface.

Attainment factor $\beta(t)$ is defined by (15) for a single three-core cable laid directly:

$$\beta(t) = \frac{-Ei\left(-\frac{D_e^2}{16t\delta}\right)-\left[-Ei\left(\frac{L^2}{t\delta}\right)\right]}{2\,In\left(\frac{4L}{D_e}\right)} \quad (15)$$

Where D_e is the diameter of the external diameter of duct, Ei (x) is the exponential integral function, t is equal to $3600i$, i is in hours.

$$k = \frac{W_1 T_4}{W_c(T_a T_b)+W_1 T_4} \quad (16)$$

Where W_c *is* power loss per unit length of conductor, T_a and T_b are corresponding thermal resistances, W_i is total Joule power loss in the cable per unit length and T_4 is the thermal resistance of the soil where the cable is buried.

IEC 60853-2 has been adopted by H.J. Joergense et al.[23] and M. Stojanovic et al.[29] to calculate the rating of XLPE cables based on daily cyclic load. H.J. Joergense et al. concluded that from both the temperature results for the distributed temperature monitoring systems installed on the cable systems, and the FEA models which implemented IEC 60853-2 showed that none of the cables reached their temperature limits. Paper from [29] is based on a single-core XLPE land cable exposed to different cyclic load profiles to investigate their influence on cable temperature. The author varies the thermal conductivity and diffusivity of soil, the distance between adjacent cables, temperatures of referent soil and cross-bonding of metal sheets to analyse the conductor temperature. The aim of this paper was to provide results that can be used in the estimation of cable overloading capability and the influence of cable aging when exposed to cyclic loading.

2.4.2 Finite Element Analysis

FEA [35] is a numerical calculation method which uses partial differential equations to solve problems. Compare with the early work by N. Flatabo [36], the required time to solve a FEA model has decreased substantially due to the availability of increased computational power. The FEA technique used in rating calculations has been proved viable by many researchers in the

case of directly buried [27, 28, 37, 38] cable circuits, forced-cooled cable circuits [39, 40] and 3-D joint bays within cable circuits [41]. 3-D modelling presents a larger computational burden for building and solving time when compared to 2D models [41].

The general principle of FEA [35] is as follows :

1) Divide a solution region into finite elements creating a mesh of polygons.
2) Interpolation functions, usually polynomials are used to interpolate the field variables over the element.
3) Establish the matrix equation with the unknown functions of the nodal values that relate to other known parameters.
4) All elements used for discretization must be assembled for all the element equations. Element connectivity are used for the assembly process. Boundary conditions should be imposed before solving the system.
5) Solve the finite element global equation system with direct or iterative methods. Direct methods are based on Lower and Upper decomposition (LU) and solve with one large computational step. Iterative methods are similar to conjugate gradient method and solve the solution gradually. The nodal values of the sought function are produced as a result of the solution.

FEA has proven to be more accurate than analytical methods, as it enables actual environmental conditions to be considered. It is widely used by researchers for calculating the rating of underground cables with various environmental conditions [28, 37, 38, 40, 42]. One example from M.S. Baazzim et al. [28] showed that the capability of FEA enabled the inclusion of wind speed, which had a significant impact on the rating of the cable. F.S. León et al. [38] used FEA to analyse the effects of different types of backfilling on cable ampacity. Backfilling are soils that were modified to improve its thermal conductivity property. The results shows that with a controlled backfill versus directly buried cable, the ampacity can be increased by 95% which is really significant.

2.4.3 Probabilistic Rating Methods

A probabilistic rating method is based on cable thermal parameters that exhibit random variations to derive the cable temperature. The cable thermal parameters involved are

operational loading (input power) and environmental temperature (soil / ambient variations caused by seasonal change). Traditionally, the cable temperature is calculated based on the worst case analysis of the cable parameters. However, if these cable parameters are described by their associated probability distributions evaluated on the basis of statistical data and historical records, the rating obtained from this method will be more accurate.

The general concept involves deriving probability distributions for the required cable thermal parameters, then using Monte Carlo Simulation to generate random numbers which are used to reference results from the probability distributions. A piecewise equation with sensitivity coefficients is then used to calculate all the scenarios generated by Monte Carlo simulations, producing a realistic distribution of the final cable temperature. This final result indicates whether the cable under operational conditions would, or would not reach threshold limits.

Probabilistic rating methods have been researched in the past [43-51]. The earliest work on a probabilistic rating were initiated by M. El-Kady et al [49] in 1984. The authors of [49] presented a technique for predicting the temperature rise and load capabilities of power cables based on statistical variation of various soil, boundary and loading conditions. Their final results based on probability density curve of the cable temperature indicated the cable under operational conditions did not reach threshold limits. This suggested that there was the possibility of improving current ratings.

In 1990, S.M. Forty et al. [50] employed probabilistic methods and finite element techniques to obtain accurate predictions of cable ampacities. The authors of [50] found that cable load, ambient temperature, native soil thermal resistivity and backfill thermal resistivity, all these factors exhibit statistical variations. Their probabilistic method is based on all these. The probability distributions of cable loading and ambient temperature were derived from historical records and Canada's weather records respectively. The transient thermal probe technique [52] and a micro-computer controlled thermal property analyser to obtain the thermal resistivity values of the soil and cable environment. The authors concluded that the probabilistic method for thermal analysis of loaded cables, when combined with the information gained from the cable conditions survey, has the advantage over traditional deterministic methods of quantifying the benefit/risk trade-offs, thereby contributing more useful information to the decision making process.

A study using a steady state probabilistic rating method was carried out by G. Idicula [43, 44] on a 400kV separate pipe forced-cooled underground cable system in 1991. Thermal parameters during operation were subject to random variations and it was possible to determine the probability distributions of these parameters. From his probabilistic analysis for July and December, the author confirmed that temperature limits are not reached during operation. He further illustrated that current can be further increased by up to 20% without exceeding the temperature limits. However, this probabilistic method is based on steady state conditions and assumptions are made regarding pipe outlet water temperature. Both of these suggest inaccuracies and an overrating would still expect to be calculated.

The probabilistic rating technique implemented by A.K. Blackwell et al. [47, 48] was based on transient instead of steady state conditions. Her method is based on a cyclic probabilistic method that enable ratings to be forecast for planning purposes. The loading of a cable circuit is determined by the post fault emergency rating that a cable can carry. Traditionally, this is determined by worst-case values. However, although some margin of safety is required, this results in pessimistic ratings and large reserve capacity on the circuit. This paper presented the probabilistic technique to enable this reserve to be realised by considering the variation of thermal parameters.

The reliability of the probabilistic method has been checked and validated with two existing models. Both of these use the superposition method specified in [53] and have been thoroughly tested against a real-time monitoring system where the cable loading, ambient temperature and cooling water temperature are being monitored [47, 54] . The author concluded that the probabilistic rating does not forecast ratings that are identical to those indicated by the real-time monitor as the monitor calculates ratings based on the actual ambient and water temperatures, while the probabilistic method relies on probability distributions. Also the monitor calculates its ratings based on both actual and historic cable loading while the probabilistic method assumes a constant cyclic shape. In general, the probabilistic method forecasts ratings to within +3% of those indicated by the real-time monitor. This method also showed that the ratings can be increased by 44% while remaining within the cable's operating temperature limit 88% of the time. However, there is still 12% of the time that the cable is not within the cable temperature limits. This percentage is a high risk to be considered and is too frequent for a cable to not be within the threshold limits.

H.C. Zhao at el. [51] presented a paper for establishing the probabilistic cable rating with a new technique for studying the cable thermal environment. This new technique focusses on collection of the soil thermal resistivity and diffusivity based on an online monitoring system with installed data logger systems and buried spheres. The transient sphere is a new technique for measuring the soil thermal resistivity and diffusivity as first used by [55]. This paper focussed mainly on the technique to measure the soil thermal resistivity (which is highly based on the rain fall), as opposed to the probabilistic method used.

2.4.4 Main Factors Influencing Rating for Wind Farm Cables

Weather conditions are a critical factor for wind farm location as wind speed ultimately determines the power output [56, 57]. However, since wind speed is highly fluctuating, power generated does as well. These fluctuations result in the offshore wind farm cable experiencing a load pattern that is non-cyclic and non-predictable [23].

The surrounding medium for the cable is another important factor in determining the rating of the cable [58]. According to G.J. Anders et al.[38], besides the conductor size, the thermal resistance of the surrounding medium has the greatest influence on the cable current carrying capability.

2.4.4.1 Wind Farm Power Output Data

The conductor temperature of the subsea cable is influenced by wind farm output power; which is influenced by wind speed and seasonal weather variations. The wind speed at site and the turbine power rating determine the amount of power that will be generated.

For this research, the source for the wind power output data are from Cullerin Range wind farm which is located 30km from Goulburn in southern New South Wales (NSW), Australia [59] (data obtained December 2013). It is a 30MW wind farm with 15 wind turbines and rated at 2MW each. There are other sources, one example are National Grid and Elexon Neta websites [60] which provide an aggregate wind power generation for the whole of the UK for onshore and offshore windfarms. The wind power graph for one year is shown in figure 2.5 is presented in the form of power output versus time.

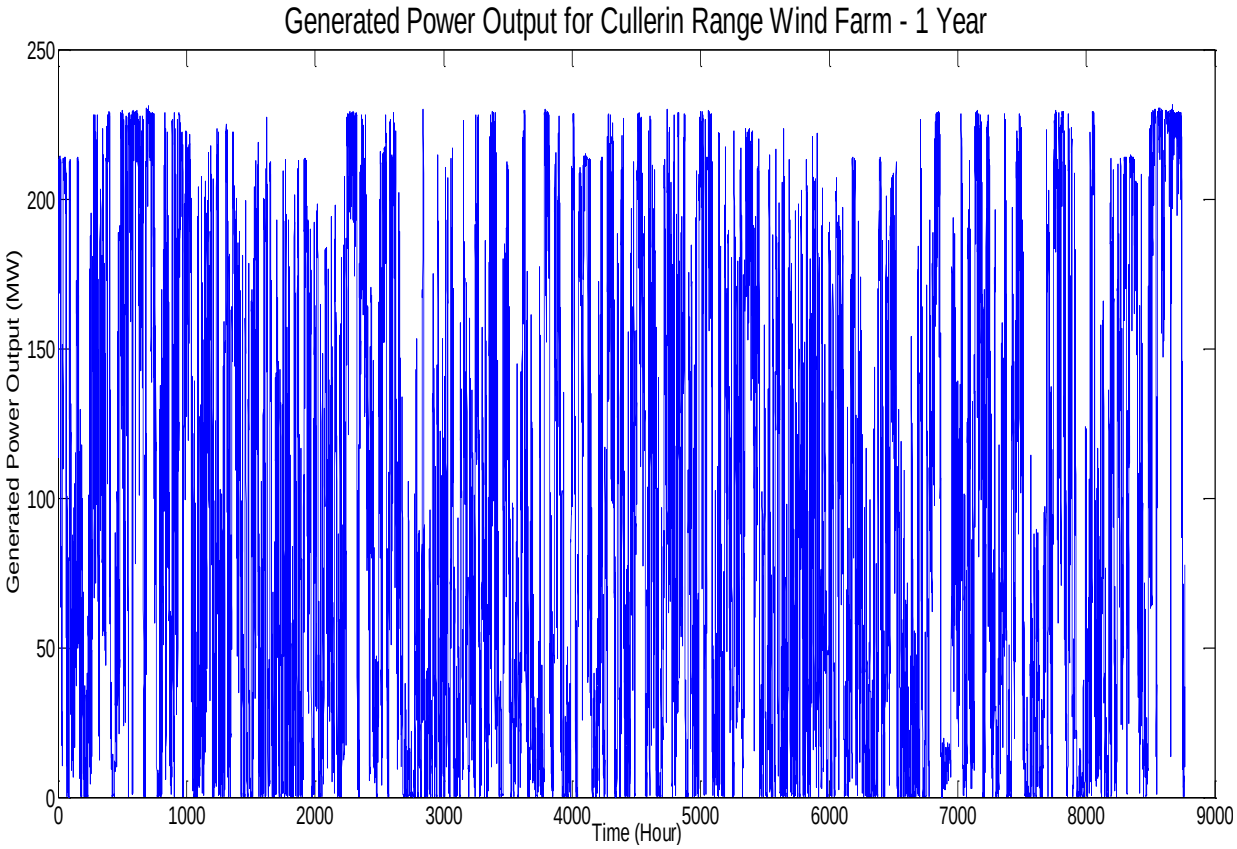

Figure 2.5**:** Example of Generated Wind Power for One Year from Cullerin Wind Farm

2.4.4.2 Environmental Ambient Data

The subsea cable goes through three different environmental medium. These mediums are soil (land/landfall section), seabed (burial for subsea section), or in air (J-tube section). This research project investigates all three sections, however the J-tube section involves the most complex set of considerations, which increases the level of difficulty for obtaining an accurate cable rating due to the cable's changing environment. The cable is enclosed in a steel cylinder which rises out of the sea to an offshore substation, so the FEA model needs to consider conduction (underwater), convection and radiation (in air), with seasonal ambient temperature variations.

2.4.4.3 Thermal Environment of Seabed

For buried cables, the two main factors that influence the rating are the soil conditions and the burial depth. Conduction and convection are the two major modes of energy transfer in soils. The thermal resistivity of soil can be defined as a function of the soil base material, the dry

density, the distribution of grain size, the compaction, the humidity and the content of organic materials [9, 61]. As per C. Savvidou [12], conduction occurs predominantly in fine-grained soils because the molecules are closer together and much more compact, this makes the energy easier to pass along. However, convection occurs more predominately in coarse-grained soils.

In most circumstances, more than 70% of the temperature rise of buried conductors are attributed to external thermal resistance [13]. The results obtained by J. Schachner [30] showed that a soil with lower thermal resistivity allowed a significantly higher current carrying capacity to that of a soil with higher thermal resistivity, in the same cross section.

For sea floor, the water temperature variations are not as much as land based. The seasonable temperature variations become smaller as the depths deepen under the seafloor.

For the landfall section, it is considered the pinch point for the export cable rating, especially where sea defences must be crossed [62] . There is a study done by J. Joergensen [23] based on two offshore wind farms in Denmark, stated that the temperature of the subsea cable is slightly higher within the first kilometre from the substation because the subsea cable runs through around 1 km of marsh and dunes before it reaches the coastline, however, this observation is site specific. Between 12 and 13km, slightly lower temperatures are observed due to the water being deeper with stronger currents and a different composition of the seabed [23].

The burial depth of the cables on land region is another factor for consideration. The impact on the current rating of the cable is lower for increased laying depth, compared with shallow installations. An increase in capacity of nearly 50% is observed between a cable buried at a depth of 1.5m and a surface laid cable [14].

2.4.4.4 Thermal Environment of J-Tubes

The J-tube is used to guide the wind farm export power cables up to a stationary platform. Its primary purpose is to protect and support the cable [63-64]. Figure 2.6 shows a sketch of a typical J-tube with seal. The requirements for the installation of the subsea cable at the host facility through a J-tube / I-tube are described in ISO 13628-5 Section 15.4 [65].

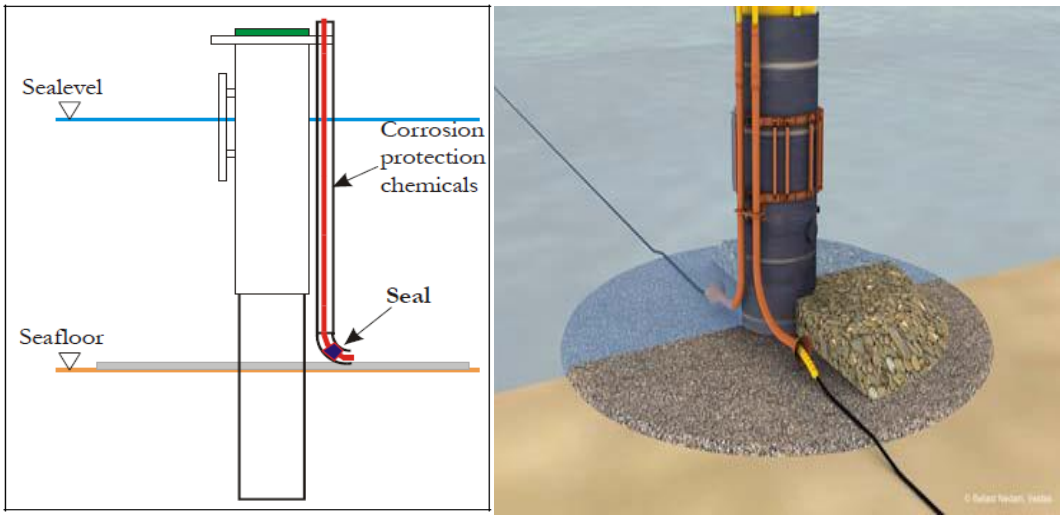

Figure 2.6: J-Tube [63]

There are 2 commonly used rating methods described in ERA 88 [19] and Hartlein and Black [66] . The heat flow path inside a J-tube can be divided into three sections according to [19].

1) Heat flow from conductors to cable surface
2) Heat flow from cable surface to J-tube
3) Heat flow from J-tube to its surroundings

Part 1 is dependent on the internal thermal resistance of the cable which can be calculated using equations from IEC 60287[4]. For parts 2 and 3, there is heat transfer due to convection and radiation. The radiation component is calculated using conventional equations with emissivity values as showed in Equation (17).

$$q'_{rad\_ext} = A_{OR}\varepsilon_R\sigma\{\theta_{OR}^4 - \theta_{surf}^4\} \quad (17)$$

Where q'_{rad_ext} is the radiation losses from the J-tube (Wm^{-1}), A_{OR} is the Lateral area of the J-tube (m^2), θ_{OR} is the Outside Temperature of J-tube (K), θ_{surf} is the Ambient Temperature around the J-tube (K), σ is the Stefan-Boltzmann Constant, 5.6703 10^{-8} ($W.m^{-2}K^{-4}$), ε_R is the emissivity of the outside surface of the J-tube(it is assume emissivity is the same on the inside and outside surface of the J-tube i.e ($\varepsilon_R = \varepsilon_{IR}$)

Heat transfer due to convection from the outside of the J-tube can be calculated using existing equations for vertical surfaces [66]. The analytical thermal convection equation is given as below.

$$Q_{conv} = h_{hb}\,(\theta_{ambinet} - \theta_{tube})) \tag{18}$$

Where Q_{conv} is the convective losses from the J-tube, h_{hb} is the heat transfer coefficient, $\theta_{ambient}$ is the surrounding ambient temperature outside tube and θ_{tube} is the temperature of the J-tube outside surface.

M. Coates [19] concluded from his experimental test results that the effect of solar radiation on the J-Tube section may reduce the current carrying capacity by approximately 26%. The test also showed that the position of the cable in the J-tube has very little effect on the current carrying capacity of the cable. The top of the tube opening doesn't influence the cable rating, however, allowing through ventilation of the tube would increase the cable rating by up to 10%. This proposition is not a practical option due to corrosion issues.

2.5 Summary

This chapter contains a review of the relevant theory of wind farm export cables, their construction and cable heat losses. The traditional cable rating methods currently being used to rate wind farm cables are presented and issues surrounding their use are discussed. Non-steady state rating methods such as FEA, cyclic and probabilistic rating techniques have shown strong indication of ways to improve the accuracy of the standard rating methods. It also explores the environmental influences which must be considered for the different sections of a cable.

Chapter 3

Model Development

This chapter describes the development of a 2D FEA model for a three-core HVAC 132kV XLPE cable using the commercial FEA software Comsol. Comsol was selected for several reasons. As well as having previous experience of using it and it being available via a University licence, its heat transfer module is easy to use and its governing equations are modifiable. It also has proven reliability and is commonly used by researchers. The FEA cable model is used for thermal analysis for the application of the non-steady state rating method, and sensitivity analysis techniques have been applied to the various model parameters, similar to those used by other researchers [31, 69] to simplify the model, thus minimising the computational size of the model without adversely affecting the quality and reliability of the results.

3.1 Properties of Cable Model

The cable properties are shown in Table 3.1. Figure 3.1 shows the full detailed cable geometry. The model developed is used for all 3 sections of the cable. The thermal analysis of the cable for steady state and transient conditions are applied for the varying environmental conditions of each cable section.

Table 3.1: Cable Parameters

Component	Material	Outer Diameter (mm)	Thermal Conductivity ($Wm^{-1}K^{-1}$)	Volumetric Heat Capacity ($MJm^{-3}K^{-1}$)
Conductor	Copper	34.3	400	3.45
Conductor Screen	Semiconducting XLPE	37.3	0.5	2.4
Dielectric	XLPE	71.3	0.286	2.4
Dielectric Screen	Semiconducting XLPE	74.3	0.5	2.4
Water Tape	Polymeric	77.3	0.286	2.4
Sheath	Lead Alloy	81.9	38.46	1.45
Semiconducting Oversheath	Semiconducting PE	86.3	0.286	2.4
Binder tape	Polymeric	189.75	0.286	2.4
Armour	Steel	200.95	18	3.8
Outer Serving	Polypropylene yarn	209.95	0.2	1.7

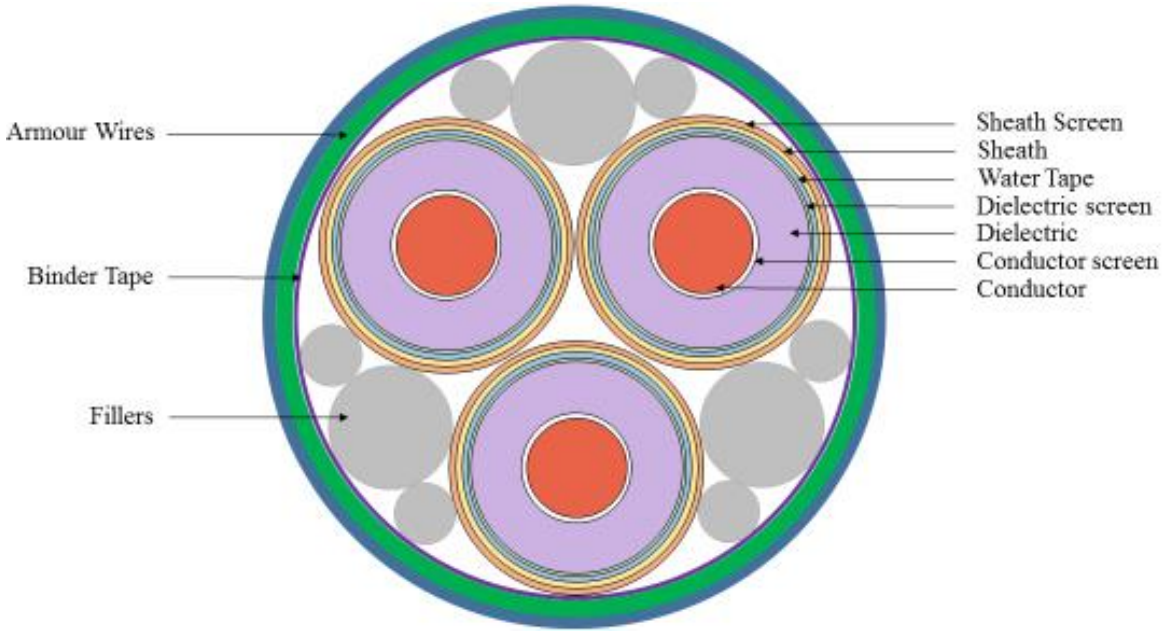

Figure 3.1**:** Fully Detailed Geometry of XLPE Insulated Three-Core HVAC Cable

In the FEA cable model, heat loss is defined using IEC 60287 and IEC 60853-2 standards. Joule loss is applied to the domain of the conductor. Dielectric loss is applied to the domain of the dielectric layer. Sheath loss is applied to the domain of the sheath layer. The armour loss is applied to the domain of every individual armour wire. Figure 3.1 shows the armour wire domain, not the individual armour wires. The rated current will be obtained by solving the

model iteratively until the conductor temperature reaches the maximum operational limit for the cable of 90°C. The fully detailed cable model is initially built in Comsol as shown in Figure 3.2. The total mesh elements for the fully detailed model is approximately 89000 elements. The mesh was created automatically using an element size set to 'normal' with little difference seen when testing with finer mesh element size.

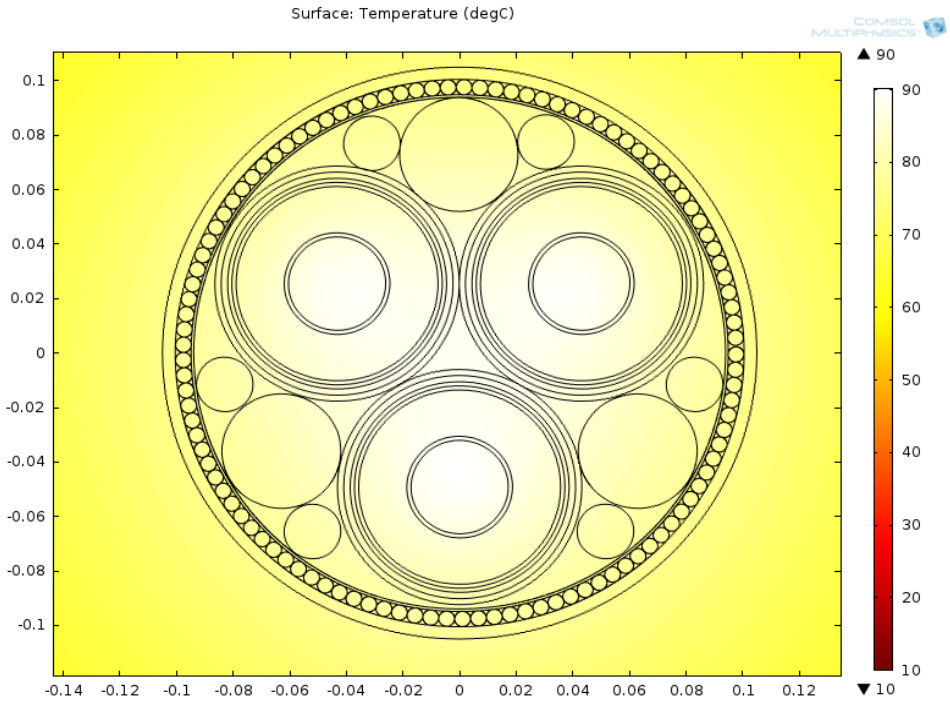

Figure 3.2: Full Detailed FEA HVAC Cable Model

In FEA, the thermal field within the cable is represented by the differential equation

$$\nabla.(k\,\nabla T) = -Q + c\,\frac{\partial T}{\partial t} \tag{19}$$

Where T is the temperature at any point (°C), k is the thermal conductivity ($Wm^{-1}K^{-1}$) , c is the thermal capacitance ($Jm^{-3}K^{-1}$), Q is the heat generation per unit area (Wm^{-2}) and t is the time (second).

For the cable model in this project, the thermal field domain for the surrounding medium (sand) is assumed to have uniform thermal properties, that is a thermal conductivity of $0.83 Wm^{-1}K^{-1}$

and thermal capacitance of 2.2$MJm^{-3}K^{-1}$. The enviromental condition for ground surface is specified isothermal at the constant ambient temperature of 15°C. The boundary conditions for both sides are set as thermal insulation meaning that there is zero heat flux crossing the boundary. The bottom boundary is specified isothermal at the temperature of 10°C [27].

The size of the sand region is determined by simulating various dimensions for the region. There are papers that suggest a typical region modelled dimension of 7m in depth [70] and ±10m in the x-axis direction from the center of the cable [40]. From the simulated results obtained, the cable temperature difference is less than 2ºC when the soil region depth is reduced from 50m to 7m. The modelled soil region in the x-axis direction from the center-line of the cable has been decreased from 10m to 7m as there is no temperature difference from this x-direction decrement. Figure 3.3 shows the thermal field domain of the cable model used for this research. The current is set at 747A. This value is obtained from the cable FEA model (below) which calculated this as the highest current without exceeding the temperature threshold limit of 90°C, for a cable buried 1m in depth, under steady state conditions.

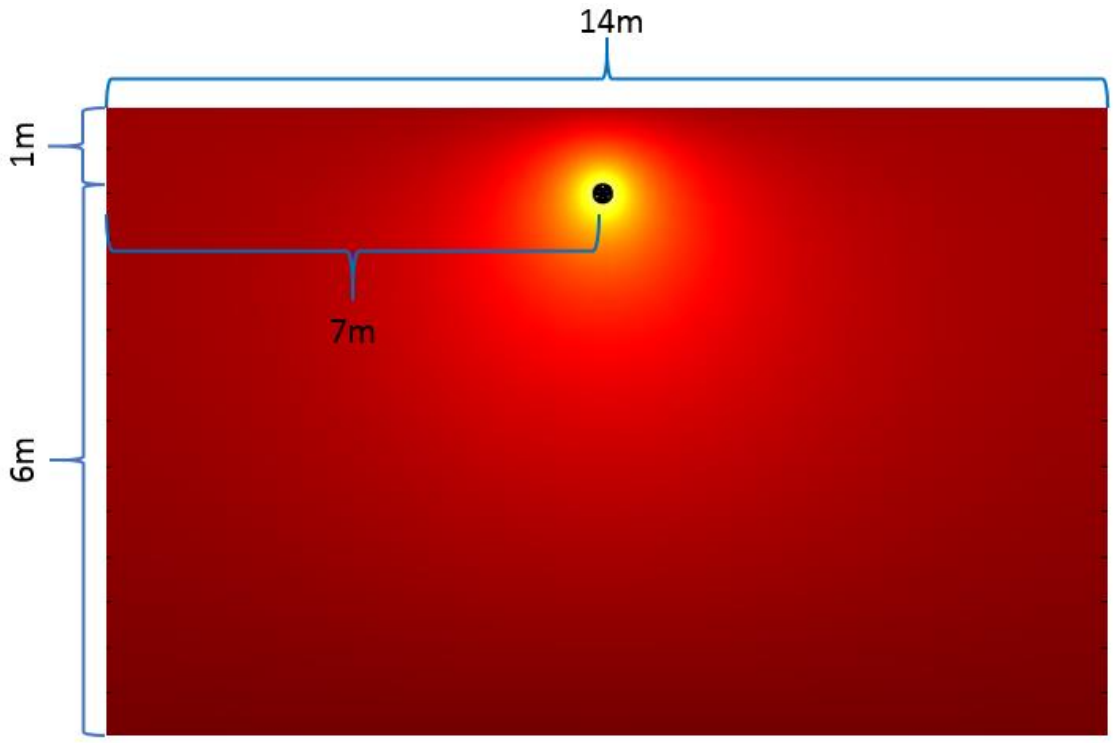

Figure 3.3: Thermal Domain for FEA Cable Model

3.2 Sensitivity Analysis for Model of HVAC Wind Farm Export Cable

This section described the sensitivity analysis performed on different parameters of the model. The model parameters will be varied one by one, in order to verify the sensitivity effect of each. The steady state load current of 747A is used for the analysis.

3.2.1 Armour

The FEA model is initially created with individual armour wires, and also with the wires merged as one domain as shown in Figure 3.4.

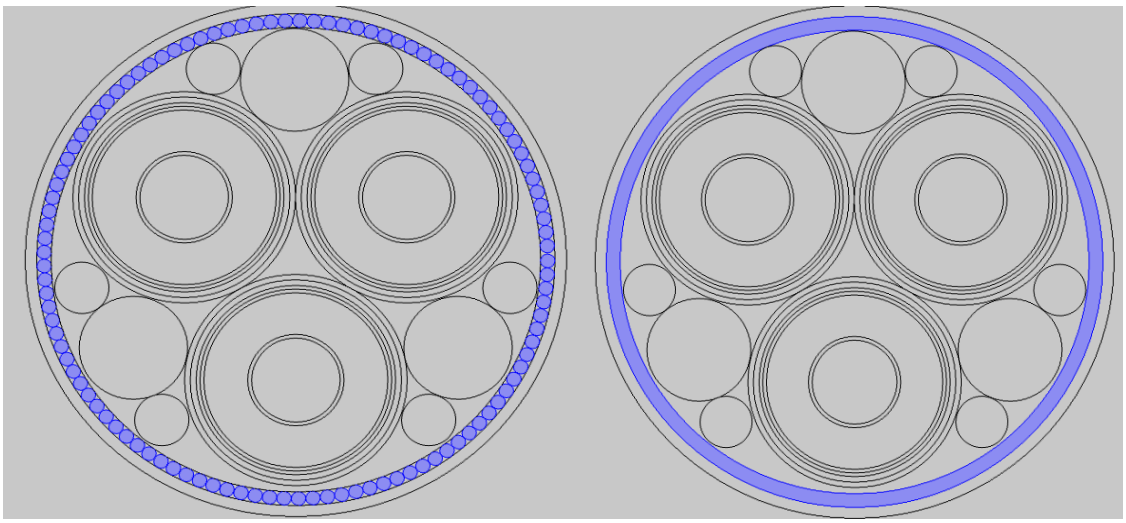

Figure 3.4: FEA Model with Individual Armour Wires (Left) and Merged Armour Wires (Right)

All the losses (that is conductor, dielectric, sheath and armour loss) and cable temperature results are tabulated in Table 3.2 for both models based on steady state and transient conditions. Different time steps of 300, 600, 1800, 3600 seconds were input into the time stepping in the FEA model. A time step for the transient model set at 1800 seconds per step provided reasonable data accuracy within the cable time constant, in an acceptable computational timeframe (1 year of data within approximately 5 hours). Time steps shorter than 1800 seconds were impractical as computational time increased significantly. The transient result showed in table (below) are the values measured at 48 hour with a rated load current.

Table 3.2: FEA Results for Model with Individual and Merged Armour Wires

Load Current = 747A	**Steady-State**			**48 Hour Transient**		
Armour Wires	**Individual**	**Merge**	**Difference**	**Individual**	**Merge**	**Diff.**
Conductor Loss (Wm^{-1})	18.30	18.30	0	16.87	16.89	0.02
Dielectric Loss (Wm^{-1})	0.391	0.391	0	0.391	0.391	0
Sheath Loss (Wm^{-1})	4.15	4.15	0	4.58	4.57	0.01
Armour Loss (Wm^{-1})	25.71	26.907	1.197	24.09	25.19	1.1
Cable Temperature (°C)	89.6	90.3	0.7	58.9	59.3	0.4

All the losses (conductor, dielectric, sheath and armour) and cable temperature from both models showed the differences are very small and therefore not significant. Concluding from the simulated results, since no appreciable loss is observed by doing so, the individual armour wires can be ignored and merged as a whole armour domain for both steady state and transient conditions.

3.2.2 Conductor Screen and Dielectric Screen

The next factor to investigate for simplifying the model are the conductor and dielectric screens. The material used for conductor screens and dielectric screens is semiconducting XLPE, which is thermally similar to XLPE. The thermal conductivity for the conductor and dielectric screens are originally set as $0.5 Wm^{-1}K^{-1}$ [71]. They are merged with the dielectric to form one domain. The thermal conductivity for the newly merged domain is set as $0.308 Wm^{-1}K^{-1}$. The total thermal resistance is calculated by summing the thermal resistance of each conductor screen, dielectric, dielectric screen layer calculated using (5). The new thermal resistivity is then calculated from the total thermal resistance obtained. Figure 3.5 showed the FEA model with conductor screen and dielectric screen (left) and merged domain for the three layers (right).

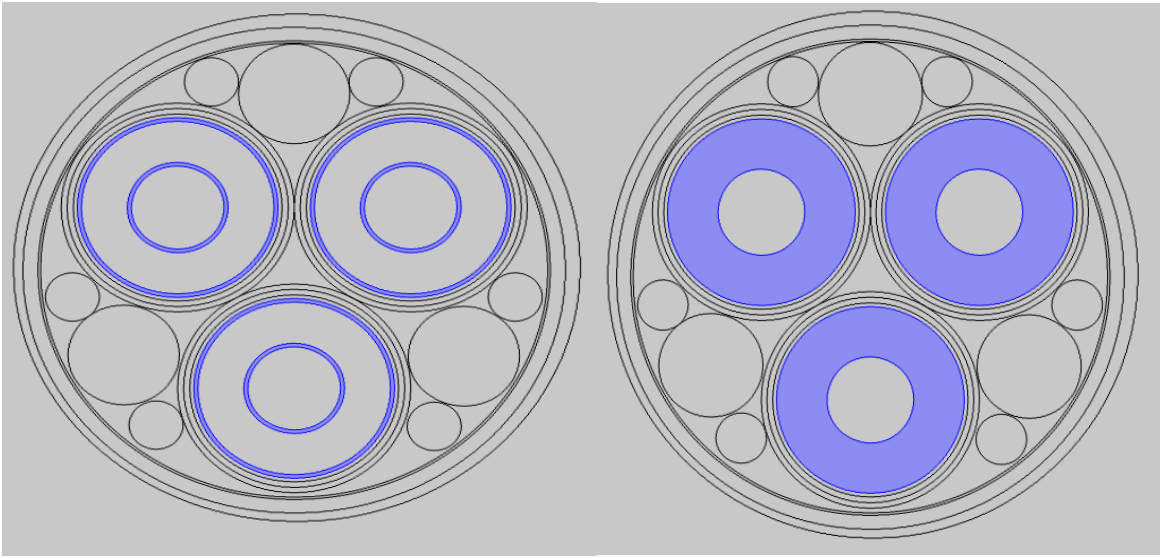

Figure 3.5: FEA Model with Conductor Screen and Dielectric Screen (Left) and Merged Domain of Conductor Screen and Dielectric Screen with Dielectric (Right)

The results obtained from FEA for steady state and 48 hour transient conditions are tabulated in Table 3.3.

Table 3.3: Results from FEA Model with Separate and Merge Conductor and Dielectric Screen

Load Current = 747A	**Steady-State**			**48 Hour Transient**		
Conductor and Dielectric Screen	**Separate**	**Merge**	**Difference**	**Separate**	**Merge**	**Difference**
Conductor loss (Wm^{-1})	18.30	18.30	0	16.89	15.94	0.95
Dielectric loss (Wm^{-1})	0.391	0.391	0	0.391	0.391	0
Sheath loss (Wm^{-1})	4.15	4.15	0	4.57	4.89	0.32
Armour loss (Wm^{-1})	26.907	26.907	0	25.19	24.09	1.1
Cable Temperature (°C)	90.3	90.3	0	59.3	59.2	0.1

There is a little difference in the losses and cable temperature observed by merging the conductor screen and dielectric screen with dielectric layer for results obtained for 48 hour transient and no difference observed in all losses and cable temperature for steady state conditions. In conlcusion, the screens can be merged as one single domain.

3.2.3 Water Tape

Water tape, which is made of a polyermic material will be merged with dieletric screen which have similar thermal properties. The thermal conductivity for water tape is set at 0.286$Wm^{-1}K^{-1}$. With this layer merged with dielectric screen, the merged domain thermal conductivity will be assumed to be same as merged dielectric domain which is 0.308$Wm^{-1}K^{-1}$. Figure 3.6 shows the FEA model with water tape(left) and merged with dielectric as single domain.

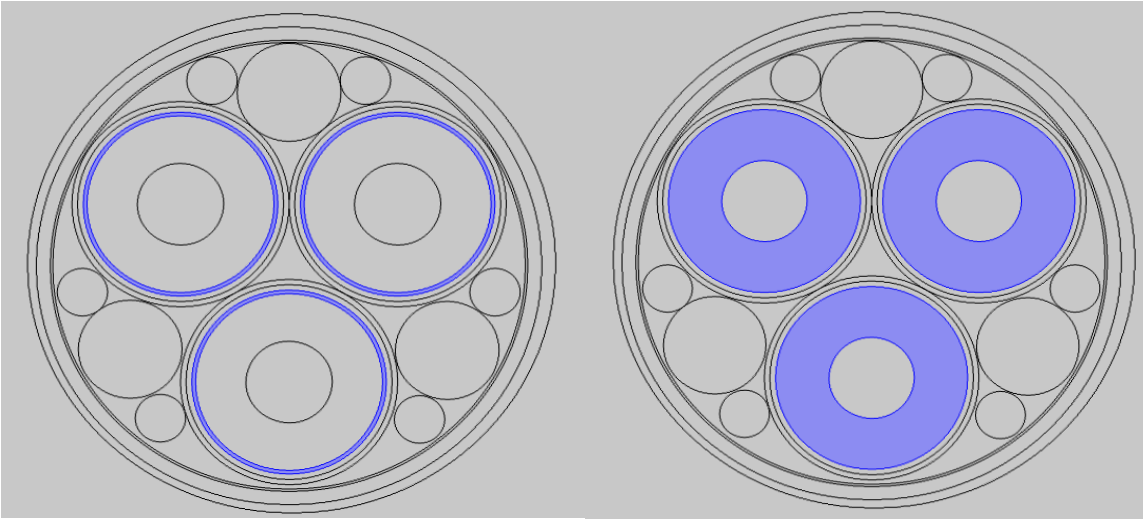

Figure 3.6: FEA Model with Water tape (Left) and Merged Water Tape with Dielectric Domain (Right)

The results obtained from FEA for steady state and 48 hour transient conditions are tabulated in Table 3.4.

Table 3.4: Results from FEA Model with Separate and Merge Water Tape with Dielectric

Load Current = 747A	**Steady-State**			**48 Hour Transient**		
Water Tape	**Separate**	**Merge**	**Difference**	**Separate**	**Merge**	**Difference**
Conductor loss (Wm^{-1})	18.30	18.30	0	15.94	15.94	0
Dielectric loss (Wm^{-1})	0.391	0.391	0	0.391	0.391	0
Sheath loss (Wm^{-1})	4.15	4.15	0	4.89	4.89	0
Armour loss (Wm^{-1})	26.907	26.907	0	24.09	24.09	0
Cable Temperature (°C)	90.3	90.3	0	59.2	59.2	0

No difference in losses and cable temperature were observed from this merging, concluding that this layer can be omitted and merged with the dielectric for steady state and transient condition.

3.2.4 Binder tape

Binder tape is another layer that can potentially be removed to simplify the FEA model. It is used to secure the fillers and cable cores together in position.

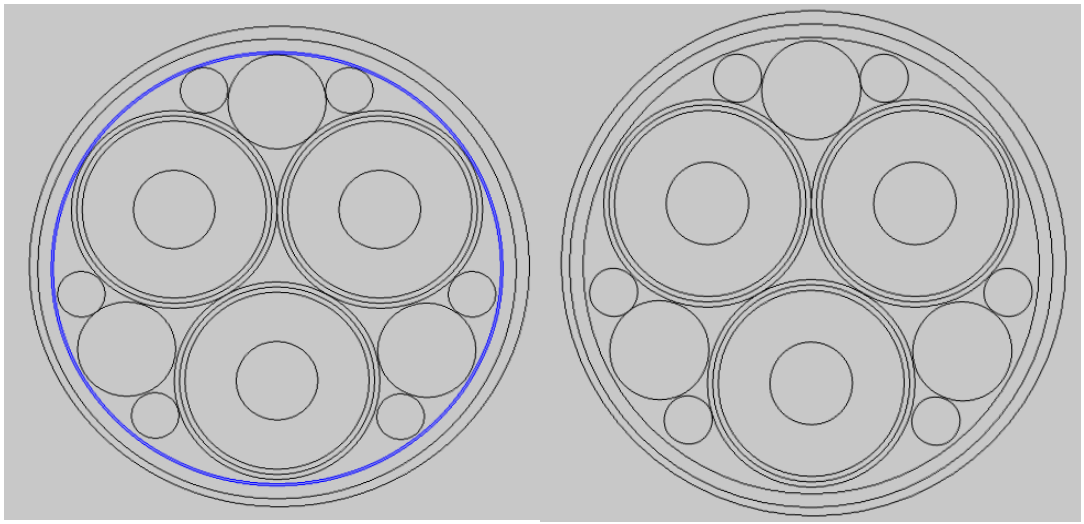

Figure 3.7: FEA Model with Binder Tape (Left) and without Binder Tape (Right)

The results obtained for the rated load current are shown in Table 3.5.

Table 3.5: Results from FEA Model with and without Binder Tape

Load Current = 747A	**Steady-State**			**48 Hour Transient**		
Binder Tape	**Include**	**Exclude**	**Difference**	**Include**	**Exclude**	**Difference**
Conductor loss (Wm^{-1})	18.21	18.27	0.06	15.93	15.97	0.04
Dielectric loss (Wm^{-1})	0.391	0.391	0	0.391	0.391	0
Sheath loss (Wm^{-1})	4.18	4.16	0.02	4.89	4.87	0.02
Armour loss (Wm^{-1})	26.90	26.90	0	24.12	24.1	0.02
Cable Temperature (ºC)	88.3	89.7	1.4	57.6	59.2	1.6

Results obtained showed little difference in cable temperature and losses, with or without the binder tape modelled. The binder tape will therefore be removed from the model for simplification.

3.2.5 Filler

Fillers are used to provide a stable circular base for the armouring [9]. They are filled at the outer interstices of the cores. Binder tape secures them together in position and armouring is then applied onto the binder tape. Fillers can be made of any recycled polymeric materials. The fillers air-gap is set as surface to surface radiation and, with surface emissivity set at 0.9. The fillers are removed from the cable model and domain are set as the fraction of area of fillers over total area of air with fillers which is calculated to be 0.576. The fraction of fillers thermal conductivity is calculated as 0.115 $Wm^{-1}K^{-1}$ and thermal capacitance is 0.979$kJ.kg^{-1}K^{-1}$ [72].

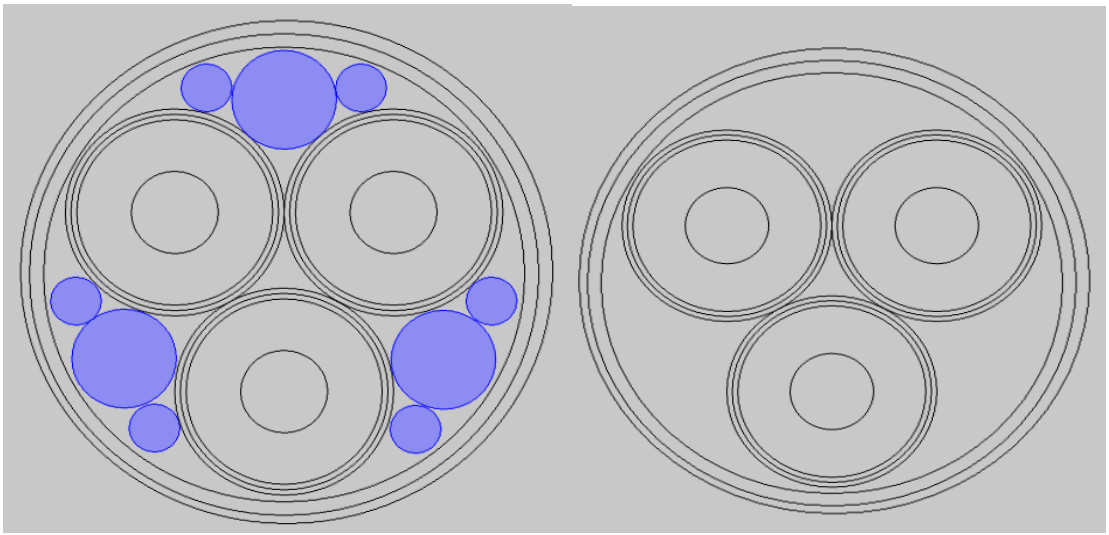

Figure 3.8: FEA Model with Fillers (Left) and without Fillers (Right)

Results obtained showed that by merging the fillers with the air domain, the effect is small enough to be deemed acceptable for the purposes of simplifying the model. The error associated with the transient temperature distribution is observed to be larger than under steady state conditions, however the difference between the cable losses are still very small and the cable conductor temperature difference is less than 2°C. The losses seen can be considered within acceptable levels and fillers will therefore be merged with air for the model.

Table 3.6: Results from FEA Model with and without Fillers

Load Current = 747A	**Steady-State**			**48 hour Transient**		
Fillers	**Include**	**Exclude**	**Difference**	**Include**	**Exclude**	**Difference**
Conductor loss (Wm^{-1})	18.27	18.32	0.05	15.97	16.08	0.11
Dielectric loss (Wm^{-1})	0.391	0.391	0	0.391	0.391	0
Sheath loss (Wm^{-1})	4.16	4.14	0.02	4.87	4.86	0.01
Armour loss (Wm^{-1})	26.905	26.909	0.004	24.1	24.08	0.02
Cable Temperature (°C)	89.7	90.2	0.5	59.2	60.9	1.7

3.2.6 Final FEA Cable Model

Having completed the sensitivity analysis, the final FEA model used for the thermal analysis of the cable system is showed in figure 3.9. It consists of the following elements: conductor, conductor screen, dielectric, dielectric screen merged with water tape, sheath, oversheath, armour wires merged as one domain, and outer serving. Table 3.7 compares the difference between the full the detailed FEA model and the final simplified model. Figure 3.10 showed the FEA results obtained for final simplified version model based on steady state condition.

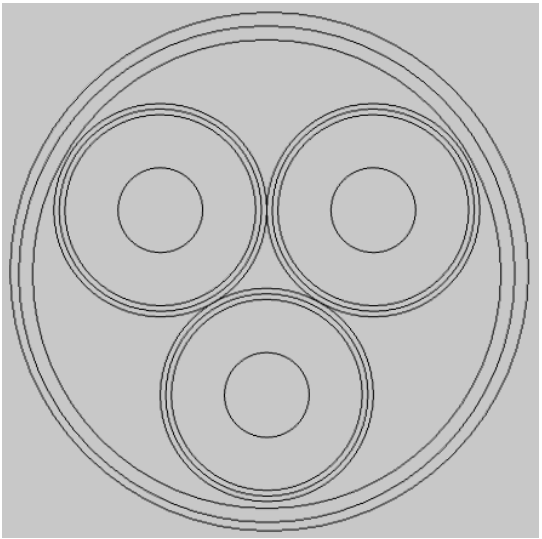

Figure 3.9: Final FEA Model of HVAC Wind Farm Cable

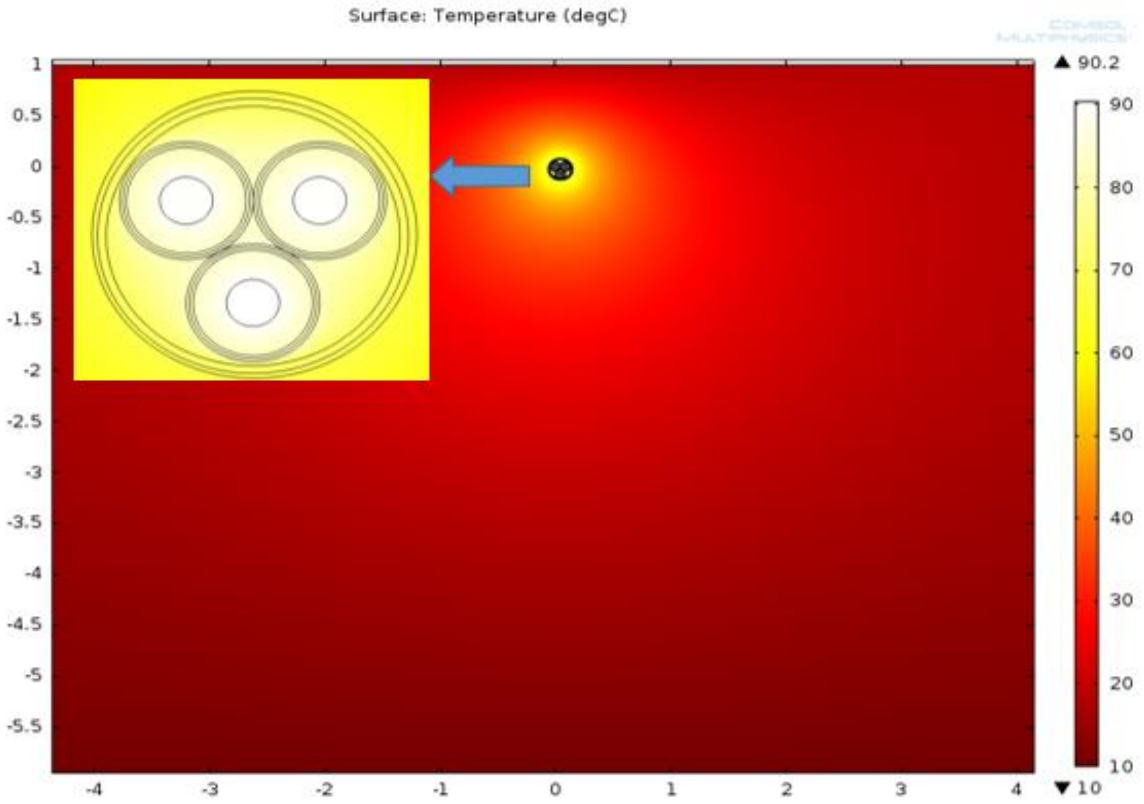

Figure 3.10: FEA Results of Final Simplified Model of HVAC Wind Farm Cable (Steady State Condition)

Table 3.7: Results for Initial Full Detailed and Final Simplified FEA Model

Rated Current = 747A	**Steady-State**				**48 hour Transient**			
Cable Model	**Full Detail**	**Final Simplified**	**Diff.**	**Diff. (%)**	**Full Detail**	**Final Simplified**	**Diff.**	**Diff (%)**
Conductor loss (Wm^{-1})	18.27	18.32	0.05	0.27	16.87	16.08	0.79	4.68
Dielectric loss (Wm^{-1})	0.391	0.391	0	0	0.391	0.391	0	0
Sheath loss (Wm^{-1})	4.16	4.14	0.02	0.48	4.58	4.86	0.28	6.11
Armour loss (Wm^{-1})	25.71	26.909	1.19	4.62	24.09	24.08	0.01	0.04
Cable Temperature (°C)	89.6	90.2	0.6	0.66	58.9	60.9	2	3.39

The final results in table 3.7 confirm the difference in losses and cable temperature are not significant, concluding that the simplified model can be used and will produce reliable uncompromised results for both steady state and transient conditions.

3.3 Summary

This chapter describes the sensitivity analysis done on the FEA model parameters in order to simplify the model and minimise the computation time required. Parameters that were analysed include merging; individual armour wires to a single armour domain, conductor screen and dielectric screen with the dielectric, water tape and the dielectric screen. Also the binder tape and fillers were analysed when present and removed from the model.

The results showed that the model can be simplified by using a single armour domain, combining conductor screen, dielectric, dielectric screen and water tape into a single domain, and removal of the binder tape and fillers, without significant effects observed.

The objective is to achieve the shortest computational solving time taken for the cable model. The full detailed model for 48 hour transient state took about 20 minutes and with the simplified model, the solving time is reduced to just 4 minutes.

Chapter 4

Cyclic Rating Methodology

This chapter applies conventional cyclic rating methods as defined within IEC60853-2 to analyse the effect of different flat-top cyclic load cycles on the thermal performance of the cable model built in Comsol. Cigre [53] states that the maximum current rating of a cable can be based on a load that is repeated cyclically in a sequence of steps. The cyclic rating changes for different sequences and cycle periods.

4.1 Modelling of Each Cable Section

The route for an offshore wind farm cable commonly includes 3 defined sections on its route from the land based substation to the offshore windfarm. This section describes the FEA model developed for each section. All cables are run from cold; that being the uniform initial temperature for a cable sections respective ambient condition. All models run a step size of 1800 seconds, proven in chapter 3 to be a time step with acceptable computational time and uncompromised results.

4.1.1 Subsea Section

The cable is buried under the seabed. The FEA model detailed in chapter 3.1 is configured for a burial depth of 1 metre. The top boundary of the sand box is set with an isothermal temperature of 18°C, which is the maximum seabed temperature for summer months according to UK Met Office (POLCOMS) data [72].

4.1.2 J-tube Section

A modified 2D FEA model is built based on a cross section cut perpendicularly across the air section of the J-tube encasing the cable.

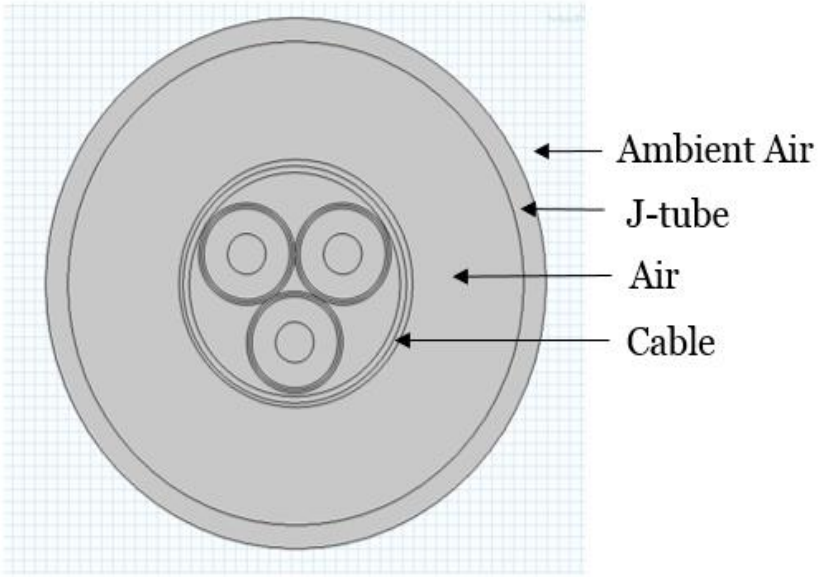

Figure 4.1: FEA Model of J-Tube in Air Section

Below are the main heat flow mechanisms to consider for the model [62].

- Convective heat transfer from the cable surface to the inner of J-tube,
- Radiative heat transfer from the cable surface to the J-tube,
- Convective heat transfer from the J-tube to the ambient environment,
- Solar gain on the J-tube surface

Steel is set as the J-tube material with a thermal conductivity of 43 $Wm^{-1}K^{-1}$ and heat capacity of 3.8 $MJm^{-3}K^{-1}$ [14]. The thickness of the steel is 20mm. The cable is centred in the middle of the J-tube by setting a 100mm air gap around the circumference of the cable surface towards the inner wall of the J-tube.

The heat loss mechanism from the conductor to the cable surface is according to IEC 60853-2 [34] standards and has been detailed in chapter 3. From the cable surface towards the inner wall of the J-tube, convective heat flux is set by using a boundary heat source. Implementing natural convection in the FEA model is believed would require an extremely long computational time. Studies were not undertaken to investigate any loss of accuracy when natural convection was not modelled, due to this analytical approach being used by several other researchers and as such viewed as the general approach [66, 73]. A negative heat flux is defined on the cable surface as shown in Equation (20), it represent the removal of heat flux from the cable surface

and transfer the energy to the inner wall of the J-tube. Since energy cannot be created or destroyed, to balance the thermal energy within the model, the heat removed from the cable surface must be placed on the J-tube boundary.

Equation (20) describes the heat flux transfer from the cable surface to the inner wall of the J-tube.

$$Q_{conv,cable} = - (h_{int} (\theta_{cable} - \theta_{tube})) \quad (20)$$

Where h_{int} is the heat transfer coefficient of the cable surface ($Wm^{-2}k^{-1}$), θ_{cable} is the temperature of the cable surface (K) and θ_{tube} is the temperature of inner J-tube surface (K).

Equation (21) is obtained from Hartlein and Black [66] to calculate h_{int}.

$$h_{int} = C \left[\frac{g\beta\{ \theta_J - \theta_{IR} Ltube^3 \}}{v^2} \right]^n \quad (21)$$

Where the values of c and n can only be obtained from experimental studies [19]. Hartlein and Blacks [67] stated that:

if $10^4 \leq \frac{g\beta\{ \theta_J - \theta_{IR} \} L^{3Pr}}{V^2} \leq 10^9$; c = 0.59 and n = 0.25

else if $10^9 \leq \frac{g\beta\{ \theta_J - \theta_{IR} \} L^{3Pr}}{V^2} \leq 10^{13}$; c = 0.021 and n = 0.4

Where L_{tube} is the length of the tube (m), g is gravity (ms^{-2}), β is the coefficient of volumetric expansion (1/K), θ_J is the temperature of cable surface (K), θ_{IR} is the temperature of the inside of the riser (K), Pr is the dimensionless Prandtl number, h_{int} is the heat transfer coefficient ($Wm^{-2}k^{-1}$), v is the kinematic viscosity (m^2s^{-1}) , c and n are both constants required to determine the Nusselt number.

The heat flux obtained from the cable surface will need to be applied to the inner wall of the J-tube to obtain a balance thermal energy for the system [66]. To achieve that, the total heat flux ($Qconv, cable$) from the cable surface (S_{cable}) is calculated by integrating Equation (20) with respect to ds_{cable}. In the model, a boundary probe is set to integrate on the cable surface to obtain the total surface heat flux.

$$Q_{conv,cable} = -\int h_{int}(\theta_{cable} - \theta_{tube})\, ds_{cable} \tag{22}$$

The total heat flux, $Q_{conv,cable}$ is then divided by the surface area of the inner wall as shown in Equation (23) to obtain the heat flux density for the J-tube inner wall. A boundary probe is set to obtain the average heat flux on the inner wall of the tube.

$$Q_{conv,tube} = \frac{Q_{conv,cable}}{S_{tube\_inner}} \tag{23}$$

For radiation inside the J-tube, surface radiation is set on the boundaries of the cable surface to inner wall of J-tube surface.

For the convective heat transfer on the J-tube outer surface to its surrounding, Equation (24) is used.

$$Q_{conv,outsidecable} = (h_{ext}(\theta_{cable} - \theta_{ambient}) \tag{24}$$

Where h_{ext} is the heat transfer coefficient of the J-tube surface ($Wm^{-2}K^{-1}$), which is using equation (21) for the calculation, θ_{cable} is temperature of the cable surface (K) and $\theta_{ambient}$ is the temperature of the ambient temperature (K).

For the solar radiation on the J-tube surface, since only half of the J-tube would be irradiated by the sun at one time, the solar heat flux is set to a factor of half. The solar heat flux is quoted

as 1000Wm^{-2} from IEC60827 standard and the thermal absorptivity of the J-Tube is 0.4 according to [67]. Equation (25) is used for solar radiation

$$Q_{solar,ext} = 0.5\ \alpha\ Q_{solar} \quad (25)$$

Where α is the absorptivity of the J-tube and Q_{solar} is the Solar heat flux.

4.1.3 Landfall Section

For the landfall section setting in the model, the size of soil box is first determined by simulating various dimensions for the region. The size of the soil box is set as 14m by 30m as shown in Figure 4.2. The top surface is set as 30°C isothermal [27] which is the summer ambient temperature according to National Grid and bottom is set as 12°C isothermal [40]. The side boundary is set as thermal insulation. The steady state rating is obtained from the FEA model is 630A for the burial depth of 3metre.

For the setting in soil material, a heaviside step function of isothermal 50°C is used [74]. The thermal conductivity is set from 1 to 1.2 $Wm^{-1}K^{-1}$ and heat capacity is set from 1 to 2 $MJm^{-3}K^{-1}$ according to National Grid guidelines as shown in Table 4.1.

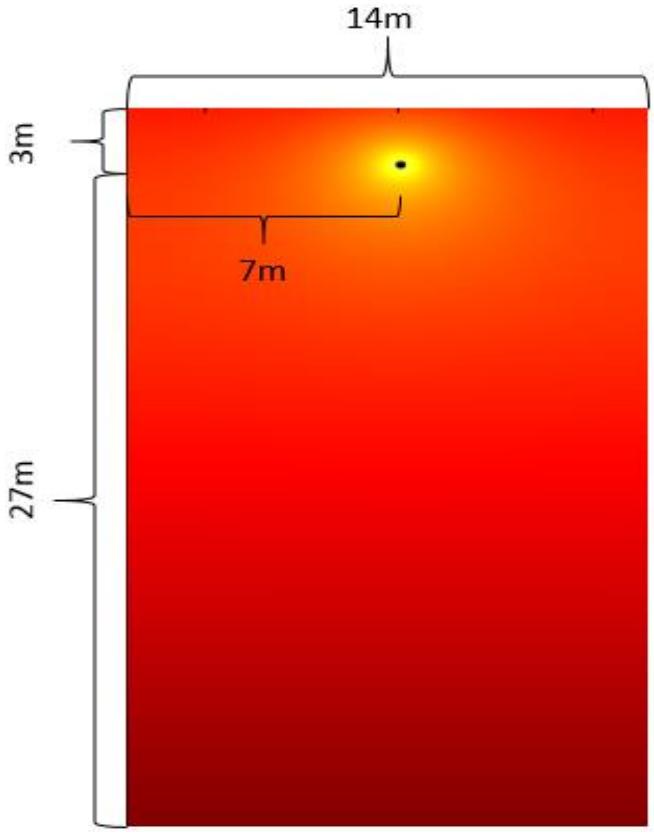

Figure 4.2: Thermal Domain for FEA Cable Model

Table 4.1: Cable Environment Thermal Resistivities [73]

Cable installation method	**Cable Environment Thermal Resistivity (K.m.W^{-1})**			
	Winter (Dec to Feb)	**Normal Cold (Mar,Apr,Nov)**	**Normal Hot (Sep, Oct)**	**Summer (May to Aug)**
Inside 50°C Isotherm				
Stabilised Backfill	1.05	1.05	1.2	1.2
Selected Sand	1.05	1.05	2.7	2.7
Unspecified	1.05	1.05	3	3
Outside 50°C Isotherm				
All materials	1.05	1.05	1.2	1.2

4.2 Daily Cyclic Load Profiles

IEC 60853-2 [34] and Electra 44 [75] states that a daily flat-topped load cycle is to be regarded as a cycle with sustained maximum current for a minimum duration of 6 hours, without any restriction on the shape of the remainder of the cycle, except that the maximum conductor temperature rise occurs at the end of the duration of sustained maximum current. The flat-topped cycle consisting of the sustained 100% rated current for x hours ($X \geq 6$) and fraction of the sustained 100% rated current for the remaining 24-x hours of the cycle.

Three different daily cyclic periods were applied to each of the 3 sections of the export cable as presented in the previous section. Each model will be run for 3 load cycles of 6 hours, 12 hours and 18 hours of high load (maximum current) during a 24 hour cycle. The remainder of each cycle will be set as low load which are 18 hours, 12 hours and 6 hours respectively. These 3 different variations of duration are chosen to evenly spread the high to low load cycle durations within a daily cycle. High load current is set at the steady state rated current for each section, being 740Aset for buried at subsea, 630A for buried at landfall and 740A for the J-tube in air section. The low load current set as 0A to represent periods when wind speed is below the wind turbine cut-in speed of $4ms^{-1}$.

4.2.1 Optimal Modelling Time

To find an optimal duration for running the models, a test was run for a 7 year period using a daily 12 hour high and low cyclic load for the buried at subsea and J-tube section. A curve is plotted from the daily maximum values to obtain the rating time. Figure 4.3 showed the 7 years of daily peak cable temperatures obtained from the model.

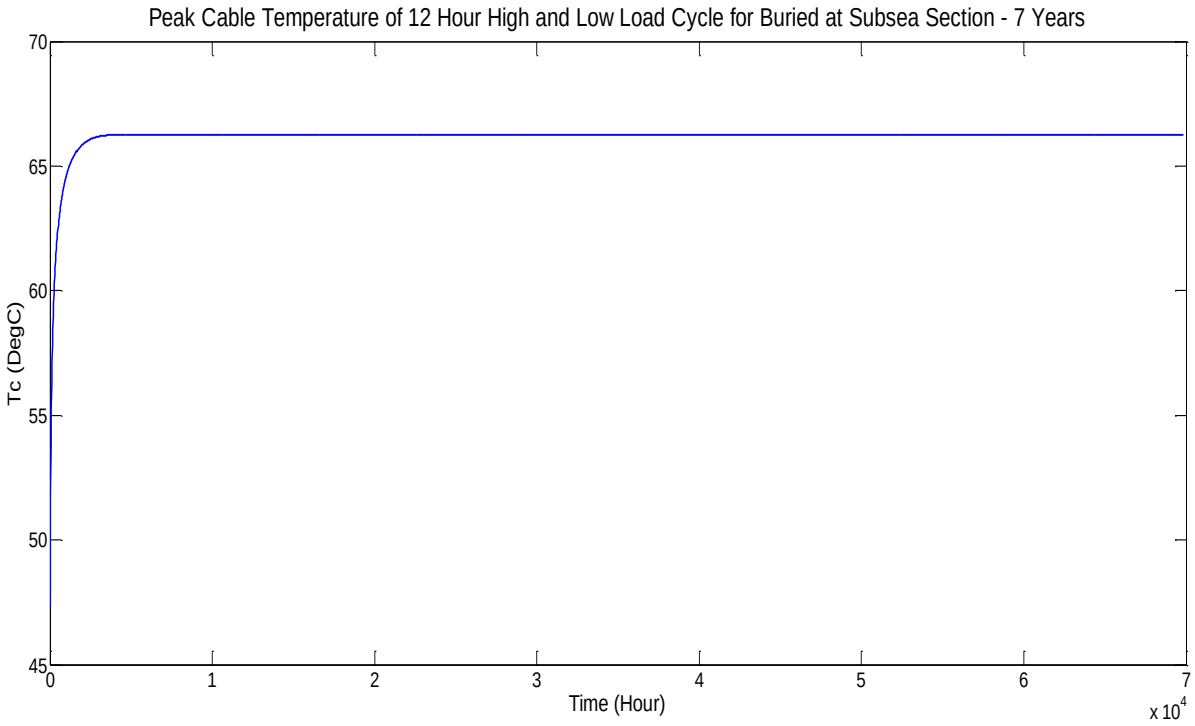

Figure 4.3: Daily Peak Cable Temperature for Buried at Sea Section for 7 Years

Figure 4.4 shows a zoom-in plot on the time when the cable temperature (Tc) stabilised, where it is observed that the cable temperature stabilised at 173 day (4125 Hour) at around 66.25°C.

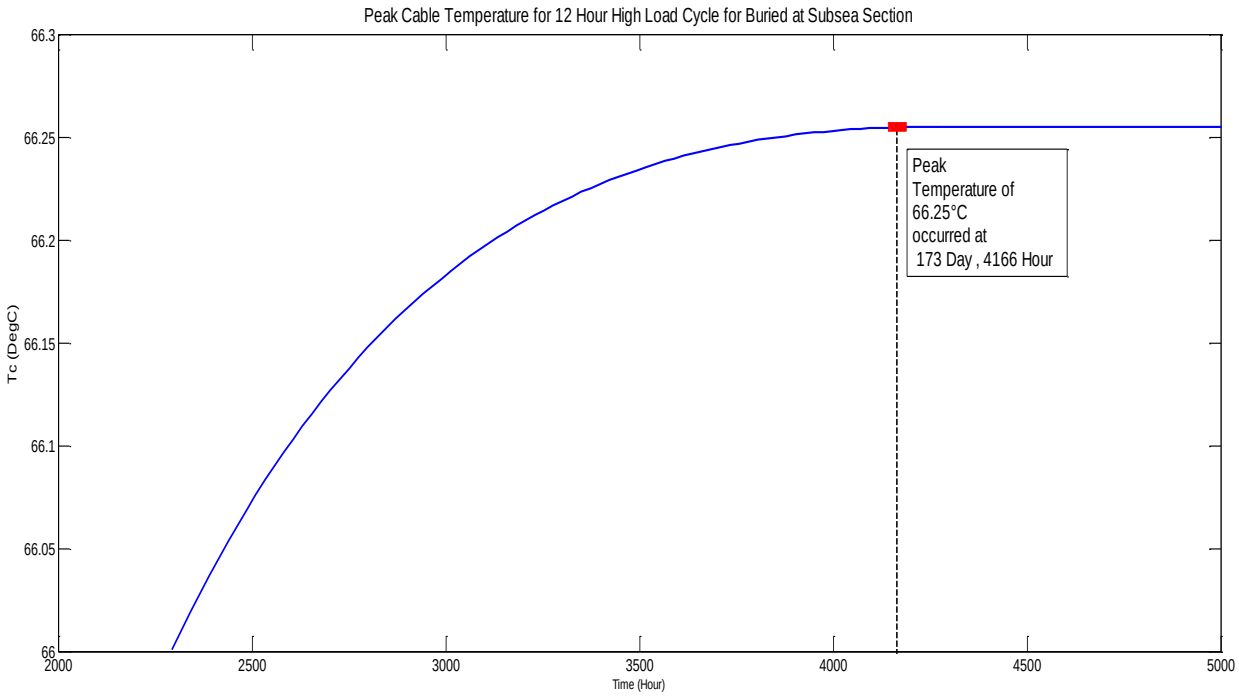

Figure 4.4: Zoom-in Plot of Daily Peak Cable Temperature for Buried at Subsea Section

The models for buried at subsea and landfall section can therefore be optimised to a duration of 6 months (182days).

A separate test for the J-tube section was run for an 8 year period to find the maximum cable temperature. From figure 4.5 which is a zoom-in plot from the 8 year focussing when the time the cable temperature are stabilised. The cable temperature stabilised at 3.5 days (82 hour) at around 82.88°C. The time to test run the J-tube model will therefore be set to one week 7 days.

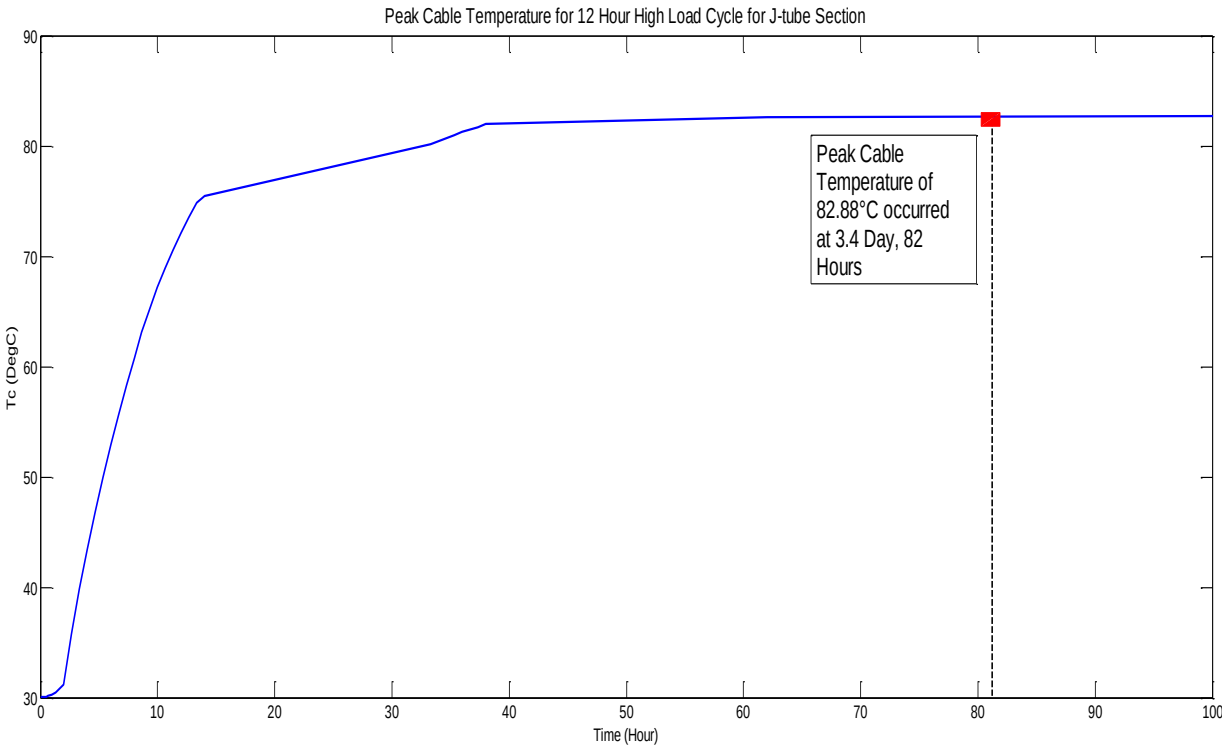

Figure 4.5: Daily Peak Cable Temperature for J-tube in Air Section

Three different cyclic loads are then applied to each cable section. Buried at sea and landfall models are run for 6 month duration and J-tube model is run for 7 days. Surface boundary temperatures are set to represent summer rating for each cable environment.

4.2.2 Simulation Results

The surface boundary ambient temperature is set to 18°C representing sea temperature. Steady state cable temperature was measured for a rated current of 740A. Current was then increased until the threshold temperature of 90°C was reached for each cycle duration. Results are compared in Table 4.1.

Figure 4.6 shows the cable temperature obtained from the 6 hour high load with 18 hour low load cycle.

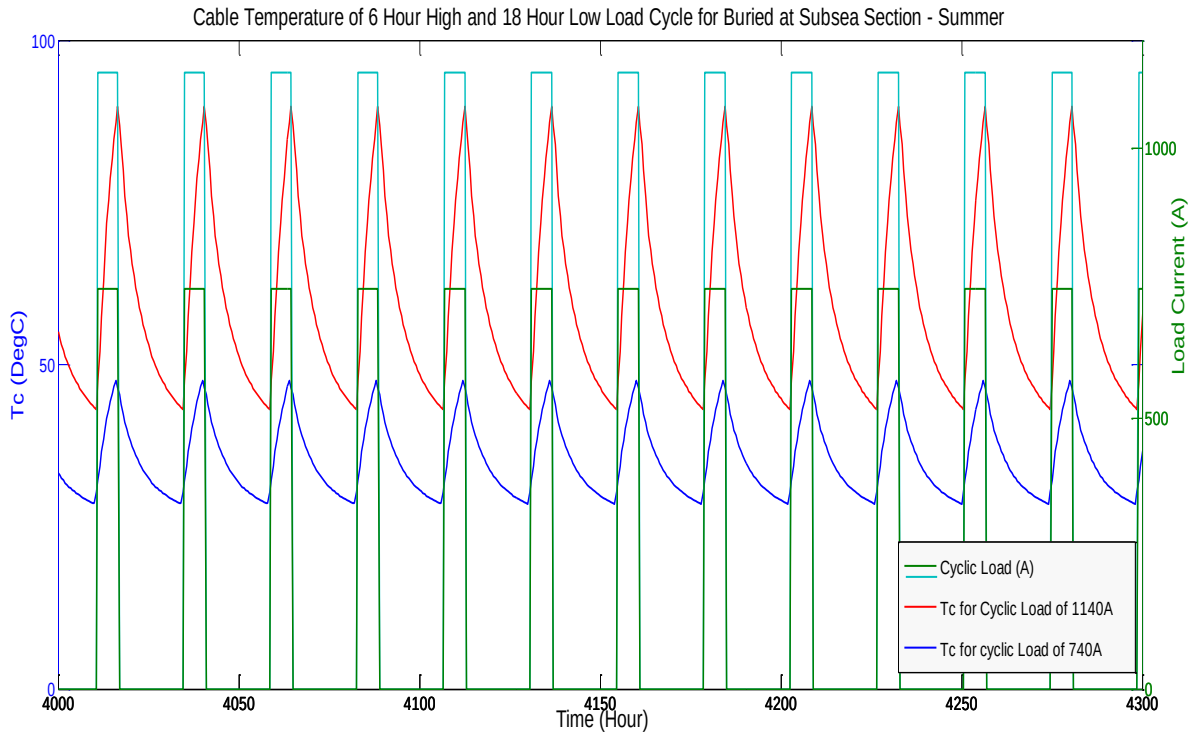

Figure 4.6: Example of Cable Temperature of 6 Hour High and 18 Hour Low Load Cycle for Buried at Sea Section

Table 4.2 summarises the cyclic loads for buried at sea section. Results show a significant increase in the cyclic rating compared to the steady state rating. The rating increased with shorter duration of high load cycle.

Table 4.2: Summary of Different Cyclic Load Cycles for Buried at Sea Section

Summary of Different Cyclic Load Cycles for Buried at Sea Section - Summer							
Cycle Duration		**Steady State**		**Cyclic**		**Rating Difference**	**Percentage Increase**
High Load	**Low Load**	**Rating**	**Temp °C**	**Rating**	**Temp °C**		
6 hour	18 hour	740A	47	1140A	90	400A	54%
12 hour	12 hour	740A	65	910A	90	170A	22.9%
18 hour	6 hour	740A	77	805A	90	65A	8.7%

The surface boundary ambient temperature is set to 30°C representing ambient air temperature above ground. The landfall section is modelled with a burial depth of 3m. Steady state cable rating was obtained at 630A. Current was increased to a threshold temperature of 90°C for each cycle to obtain the cyclic rating. Results are compared in Table 4.3.

Figure 4.7 shows the cable temperature obtained from the 6 hour high load with 18 hour low load cycle.

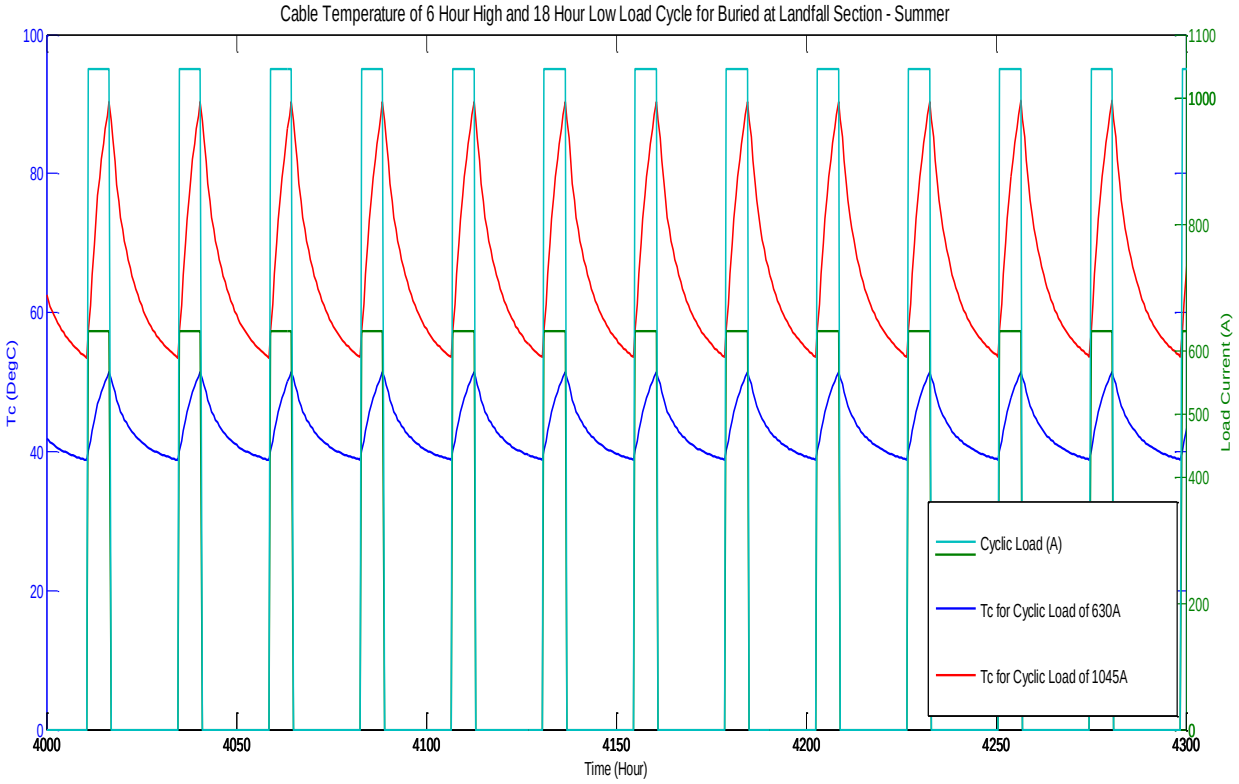

Figure 4.7: Example of Cable Temperature of 6 Hour High and 18 Hour Low Load Cycle for Buried at Landfall Section

Table 4.3: Summary of Different Cyclic Load Cycles for Landfall Section

Summary of Different Cyclic Load Cycles for Landfall section - Summer							
Cycle Duration		**Steady State**		**Cyclic**		**Rating Difference**	**Percentage Increase**
High Load	**Low Load**	**Rating**	**Temp °C**	**Rating**	**Temp °C**		
6 hour	18 hour	630A	51	1045A	90	415A	65.87%
12 hour	12 hour	630A	64	825A	90	195A	30.95%
18 hour	6 hour	630A	74	725A	90	95A	15.07%

The ambient temperature outside the J-Tube is set at 30°C as a summer rating. Steady state cable rating was obtained at 740A. Current was again increased until the threshold of 90°C was reached for the cyclic cycle. Results are compared in Table 4.4.

Figure 4.8 shows the cable temperature obtained from the 6 hour high load with 18 hour low load cycle.

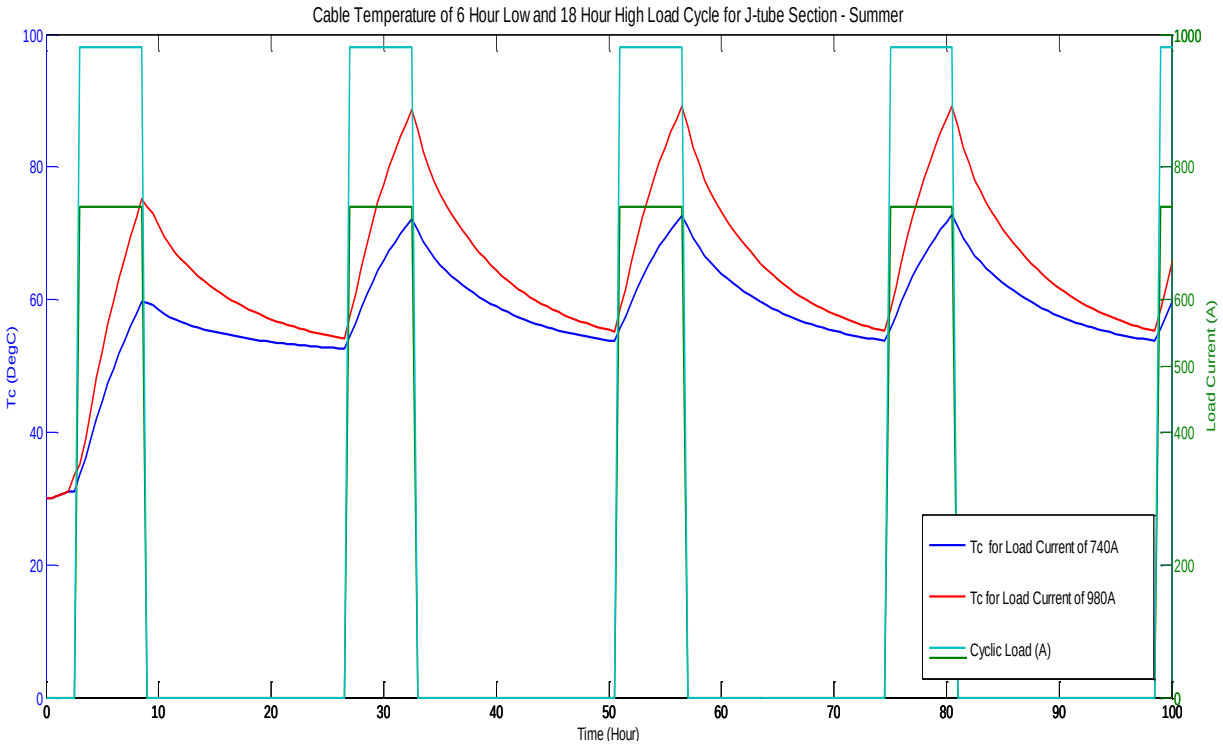

Figure 4.8: Example of Cable Temperature of 6 Hour High and 18 Hour Low Load Cycle for J-tube in Air Section

Table 4.4: Summary of Different Cyclic Load Cycles for J-Tube Section

Summary of Cyclic Load Cycles for J-Tube Section - Summer							
Cycle Duration		**Steady State**		**Cyclic**		**Rating Difference**	**Percentage Increase**
High Load	**Low Load**	**Rating**	**Temp °C**	**Rating**	**Temp °C**		
6 hour	18 hour	740A	72	980A	90	240A	32.4%
12 hour	12 hour	740A	82	830A	90	90A	12.16%
18 hour	6 hour	740A	87	760A	90	20A	2.7%

Table 4.5 summarises the simulated results obtained from all the different sections of cable.

Table 4.5: Summary of All Daily Cyclic Cycles for All Cable Sections

Comparison of Cyclic Load Cycles for All Cable Sections – Summer				
High Load Cycle Duration	**Steady State Ratings**	**Cyclic Ratings**	**Rating Difference**	**Percentage Increase**
Buried at Subsea Section Cable – Summer				
6 hour	740A	1140A	400A	54%
12 hour	740A	910A	170A	22.9%
18 hour	740A	805A	65A	8.7%
LandFall Section Cable – Summer				
6 hour	630A	1045A	415A	65.87%
12 hour	630A	825A	195A	30.95%
18 hour	630A	725A	95A	15.07%
J-Tube Section Cable – Summer				
6 hour	740A	980A	240A	32.4%
12 hour	740A	830A	90A	12.16%
18 hour	740A	760A	20A	2.7%

Results show only a 2.7% increase for rating the J-Tube section using the cyclic rating as compared to steady state rating. This indicates that the thermal time constant to reach the threshold temperature for the J-tube section is short. With such a small increment, it is not beneficial to rate the cable cyclically after more than 12 hours of high load cycle for that section.

The highest thermal time constant to reach the threshold temperature is for the buried at landfall section. It shows a significant increase in the rating for both the shortest 6 hour high load cycle and longest 18 hour high load cycle indicating that significant benefits can be obtained by rating the cable cyclically.

4.3 Non-daily Cyclic Loads Profiles

Daily cyclic load cycles are more suitable to describe load trends on domestic power cables. With wind farms the power generated is highly volatile, therefore daily cyclic loads are not a realistic way to observe the effect of thermal cable performance presented in power generation environments.

Further cyclic loads of equal duration of high and low load cycle are applied to these different sections of cable models for further analysis. A cycle of 24 hour high and 24 hour low load cycle are applied to each cable sections.

4.3.1 Simulation Results

Figure 4.9 shows the cable temperature obtained from the 24 hour high and low load cycle.

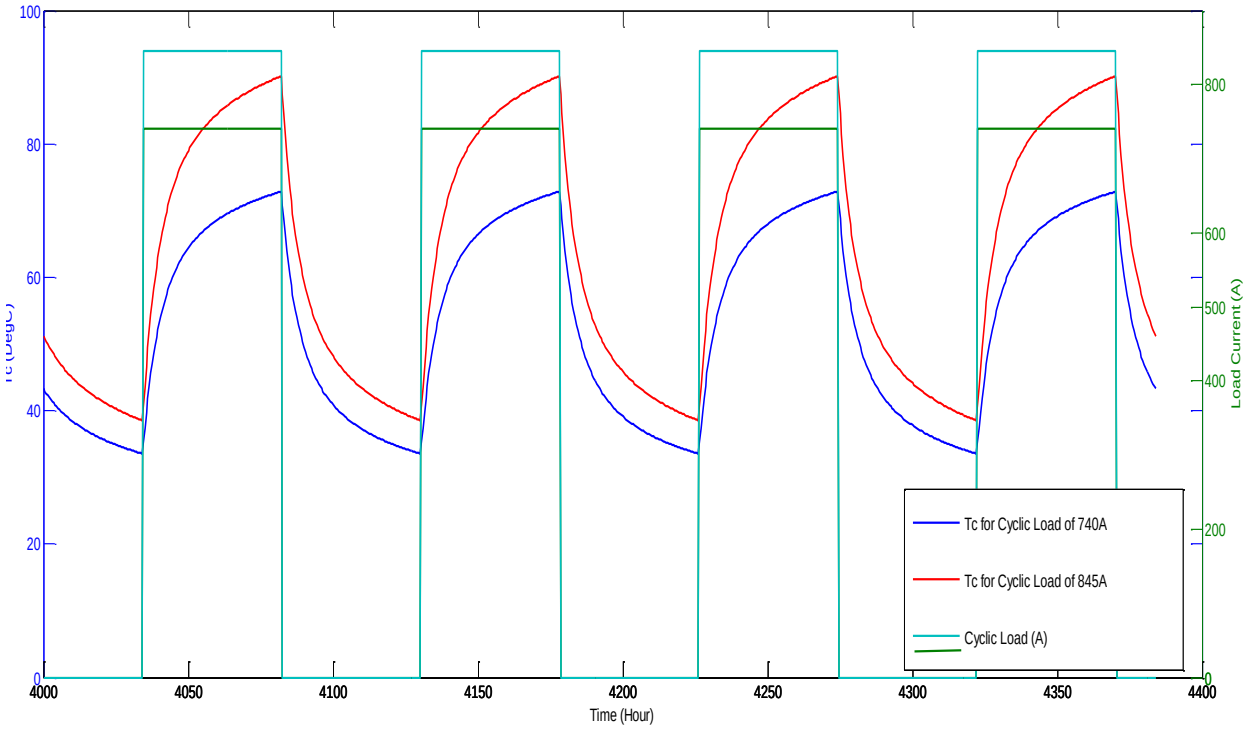

Figure 4.9: Example of Cable Temperature of 24 Hour High and 24 Hour Low Load Cycle for Buried at Sea Section

The combined results for all different sections of cable are detailed in Table 4.6.

Table 4.6: Summary of All Non-daily Cyclic Cycles for All Cable Sections

Comparison of Cyclic Load Cycles for All Cable Sections - Summer						
Cycle Duration		**Steady State Ratings**	**Temperature Reached**	**Cyclic Ratings**	**Rating Difference**	**Percentage Increase**
High Load	**Low Load**					
Buried at Subsea Section Cable - Summer						
24 hour	**24 hour**	740A	69°C	870A	130A	17.5%
48 hour	**48 hour**	740A	72°C	845A	105A	14.1%
Landfall Section Cable - Summer						
24 hour	**24 hour**	630A	66°C	790A	160A	25.4%
48 hour	**48 hour**	630A	69°C	770A	140A	20%
J-Tube Section Cable - Summer						
24 hour	**24 hour**	740A	87°C	760A	20A	2.7%
48 hour	**48 hour**	740A	89°C	745A	5A	0.6%

From the results shown, the J-tube section with the 48 hour of high and low load cycle showed only 0.6% increase of the cyclic rating as compared to steady state rating. With a 24 hour load cycle, the increase in rating is not significant staying at 2.7%, supporting the conclusion obtained for the daily cycles, that there is no benefit to rating the J-tube section for a cycle of more than 12 hour high load duration due to its short thermal time constant.

For buried at landfall section, there is a significant increase in the rating with a good percentage of 20% for a 48 hour high load cycle. For buried at sea section, it also shows good increase of 14.1% for the same cycle duration.

Results obtained from the FEA models based on daily and non-daily cyclic loads show that there is potential to rate the cable cyclically for buried at sea and landfall sections due to the long thermal time constant. For J-tube section, it is only beneficial if the high load cycle is less than 12 hour period.

4.4 Summary

This chapter describes using FEA models with conventional cyclic rating methods to analyse the effect of different flat-top cyclic load cycles on the thermal performance of the cable model. The development for 3 FEA cable sections running from the land based substation to the offshore windfarm are presented in this chapter. The 3 defined cable sections are buried at sea, landfall and J-tube in air sections. Three different daily and two longer periods (of more than 24 hours) cyclic load profiles are applied to all the cable sections. The simulation results obtained from the models have been analysed.

There are promising results obtained which suggest that using cyclic rating can substantially increase the rating for buried landfall and sea section. For J-tube section, it is only beneficial if the high load cycle is less than 12 hours.

Chapter 5

Risk of Cable Temperature Exceedance

This chapter utilises the normalised wind power data from Cullerin Range wind farm and applies it to the FEA model for the landfall section. The wind farm data is served as an example to analyse the risk of exceedance for designing the cable system using cyclic methodology.

5.1 Reference of Wind Farm Data

From chapter 4, it was observed that buried cable sections, especially those buried at landfall sections, have a long thermal constant as compared to the j-tube in air section. The landfall section is frequently considered to be the thermal pinch point for the wind farm cable. The use of cyclic rating for the buried at landfall section will definitely benefit the cable system, because the long thermal time constant allows us to test cycles of varying lengths over long periods with the potential for obtaining substantial increase in ratings without ever reaching steady state conditions. The greater the difference between the cycle increase period ('on time') and the thermal time constant, the greater potential increase in rating will be seen.

To further analyse the reliability of sizing a cable system using a cyclic loading method, 1 year of normalised Cullerin Range wind farm power data are scaled with steady state load (630A) and applied to the landfall FEA model set in summer ambient temperature of 30°C and buried at 3m in depth.

This will serve as an example to demonstrate the risk that the peak cable temperature obtained from cyclic methods will exceed that obtained from the wind farm.

The data for 1 full year wind farm load current from Cullerin Range wind farm are shown in Figure 5.1. The data received in Excel format was exported as a tab delimited text file and imported to Comsol using the Interpolation function. Once loaded, heat loss equations were manually modified to run the imported dataset.

In order to find the stabilising point where the cable temperature reaches a constant maximum, a dataset spanning several years needed to be created. Estimating it would require several years to see stabilisation of the cable temperature, an initial test period of 7 years was chosen. Fewer years may not have shown conclusive repetition and more would have increased computation time.

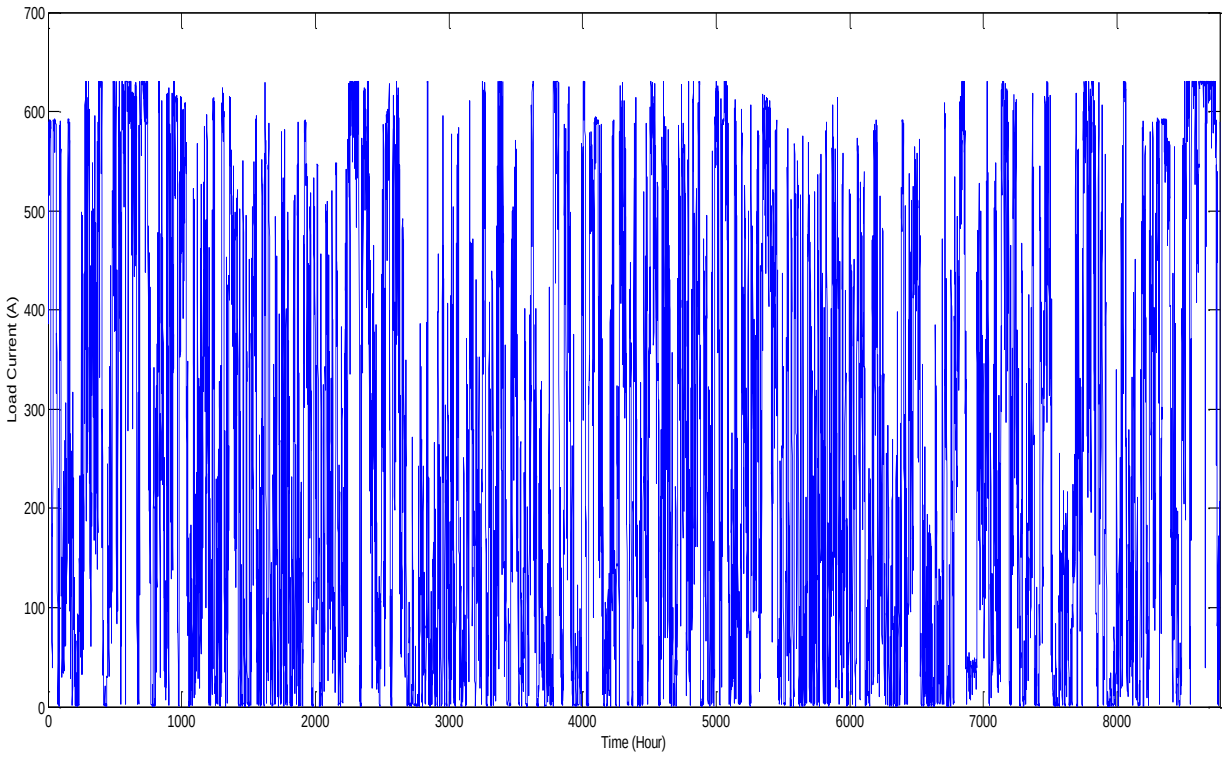

Figure 5.1: Load Current of Cullerin Range Wind Farm for 1 Year

Figure 5.2 shows the histogram of 7 years of wind farm load current data from the Cullerin Range wind farm showing that the 2 highest frequency load ranges are 0-50A and 600-630A (approximately 25% and 14.5% of total loads respectively). It should be noted that 0-50A range would also possibly include any outages during the period, for which no further information is available from the test data set.

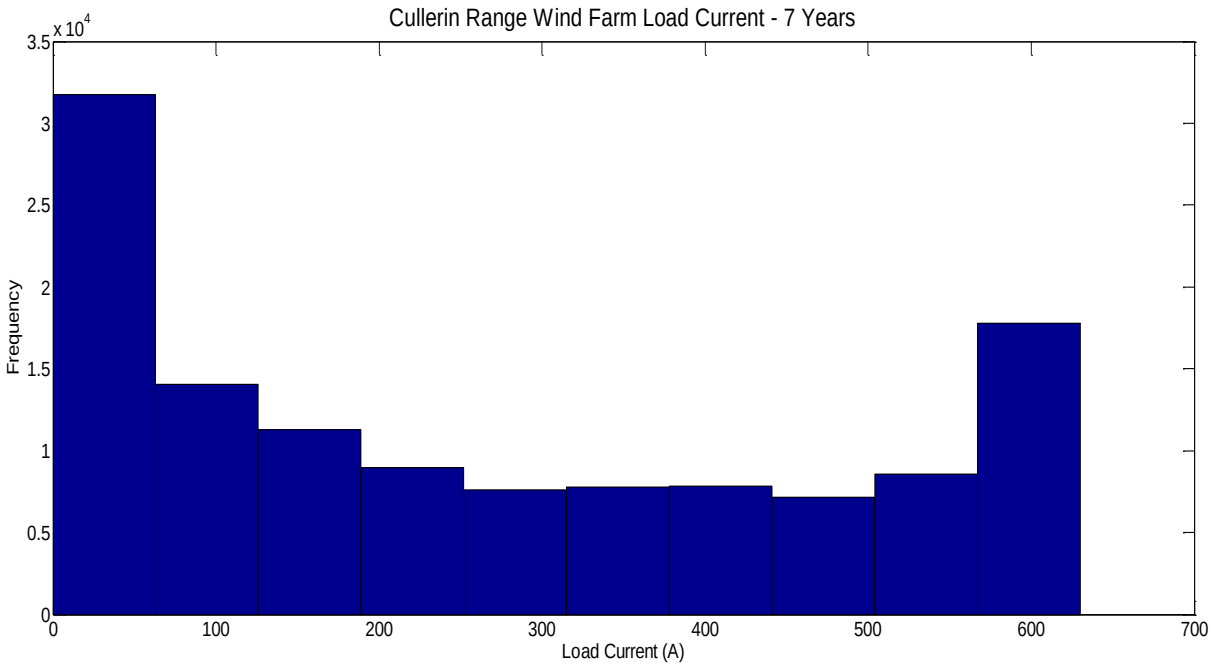

Figure 5.2: Histogram showing Load Current of Cullerin Range Wind Farm for 7 Years

The 7 years of load current are input into the FEA model for landfall section to obtain the cable thermal response. Figure 5.3 shows the thermal response of the cable to the wind farm load current. It can be noted that the highest cable temperature does not reach the cable limits of 90°C.

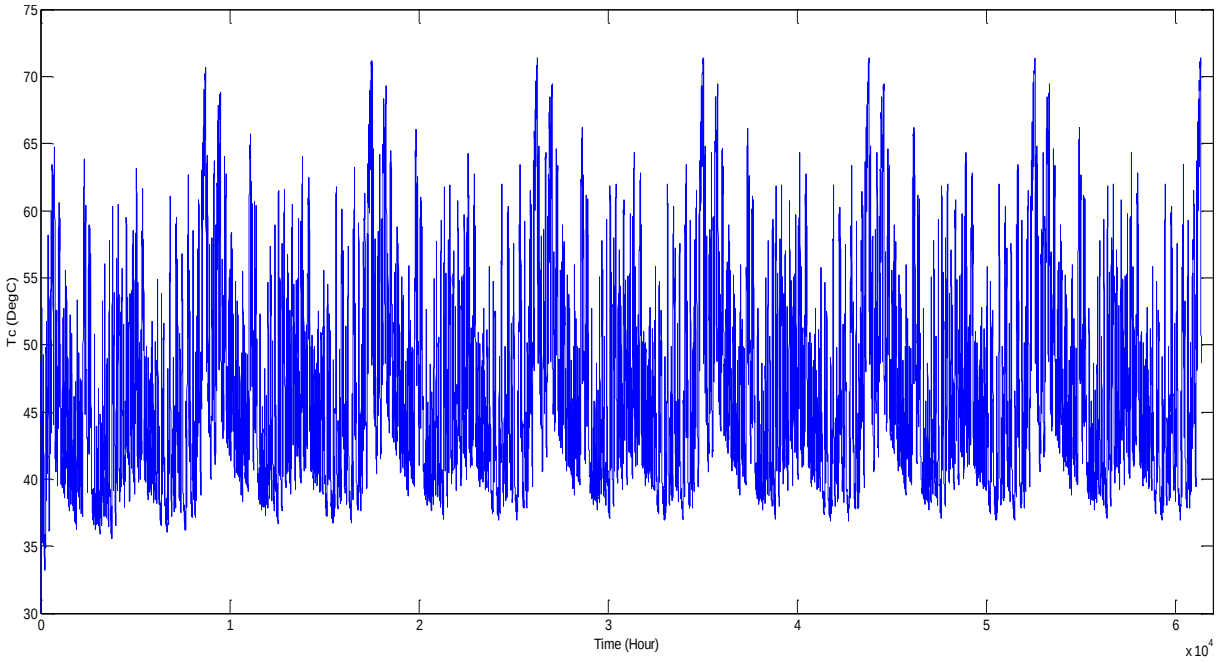

Figure 5.3: Tc (°C) of Cullerin Range Wind Farm for Landfall Section for 7 Years

5.2 Peak Cable Temperature

This section reviews the 7 years of cable temperature obtained for the landfall model. The peak cable temperature is almost reached after year 1, with the peak temperature finally stabilising at year 4.

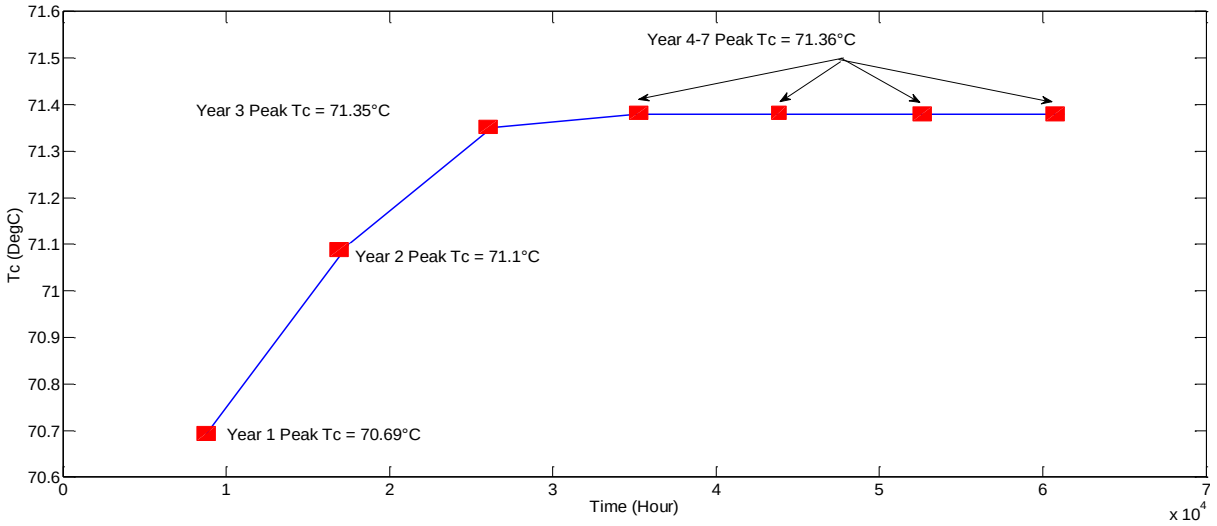

Figure 5.4: Peak Cable Temperature Per Year of Cullerin Range Wind Farm for Landfall Section for 7 Years

Figure 5.5 shows the resulting cable temperature and load current obtained from the FEA landfall model over a 1 year period. Year 4 is used as the Tc has peaked.

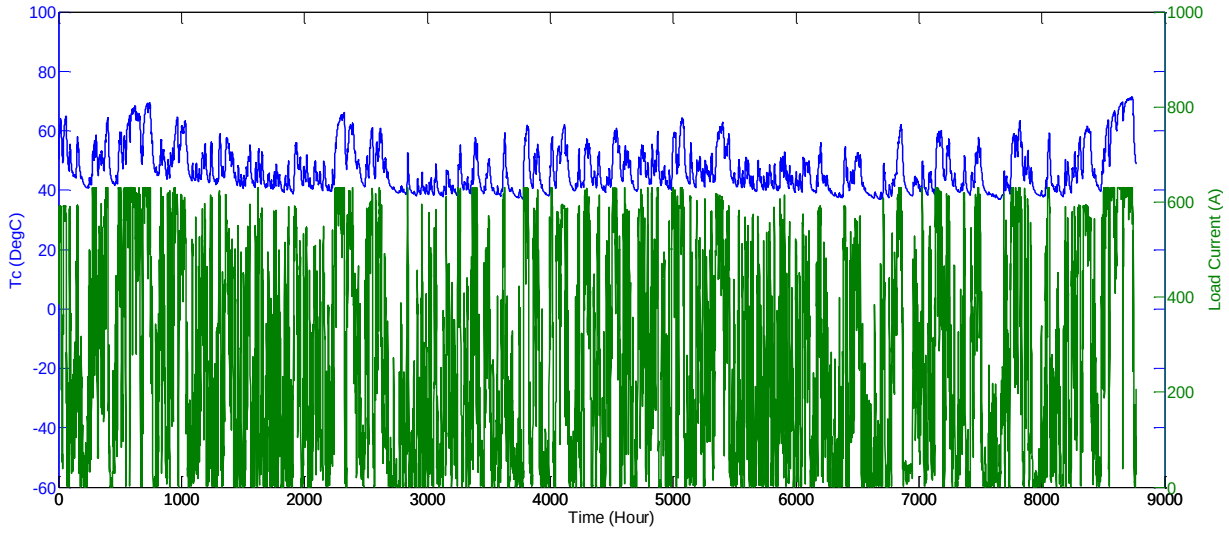

Figure 5.5: Tc Vs Load Current of Cullerin Range Wind Farm for Landfall Section

All the maximum cable temperatures from the individual cycles are selected during the 1 year data, along with the load current when these peak Tc occurred. Peak temperatures were established by selecting those Tc that are preceded and followed by a lower temperature (indicating the peak of a cycle). The corresponding load current was then taken for every cycle peak.

Figure 5.6 shows a scatter plot of these selected peak cable temperatures and its corresponding load current. It is observed that the peak Tcs and their corresponding load current have an exponential growth trend of the form:

$$f(x) = a*\exp(b*x)+c*\exp(d*x) \tag{26}$$

The full exponential equation obtained from plot can be stated as:

$$f(x)=37.85 \exp(0.000377 *x) + 0.1691 \exp(0.007113 * x) \tag{27}$$

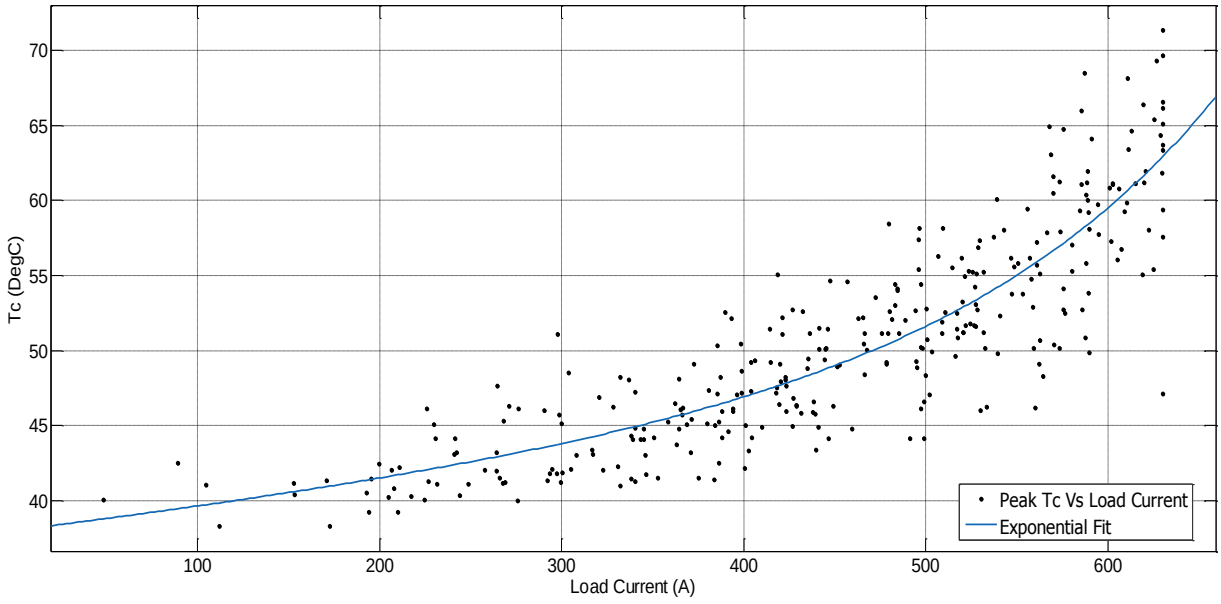

Figure 5.6: Peak Tc Vs Load Current of Cullerin Range Wind Farm for Landfall Section

5.3 High and Low Load Cycle Widths

From the one year load current obtained from the Cullerin Range wind farm, high and low loads are determined by taking the steady state rating for the landfall section (630A), and using the midpoint current value (315A) as the division between high loads and low loads. Any value in the range of 315A to 630A is considered a high load (630A) and anything from 0A to 315A a low load (0A). The current dependent heat loss is proportional to I^2R, whereby if the load is reduced by half, the heat loss is reduced by factor of 4. This would indicate that the heat loss generated at 315A is only 25% of the total heat output. The load current of 315A was applied to the steady state FEA model with a total cable heat loss obtained at 16.08Wm^{-1} which equates to a maximum heat loss for low loads. This is considered low heat loss compared to 65.44Wm^{-1} obtained at 630A.

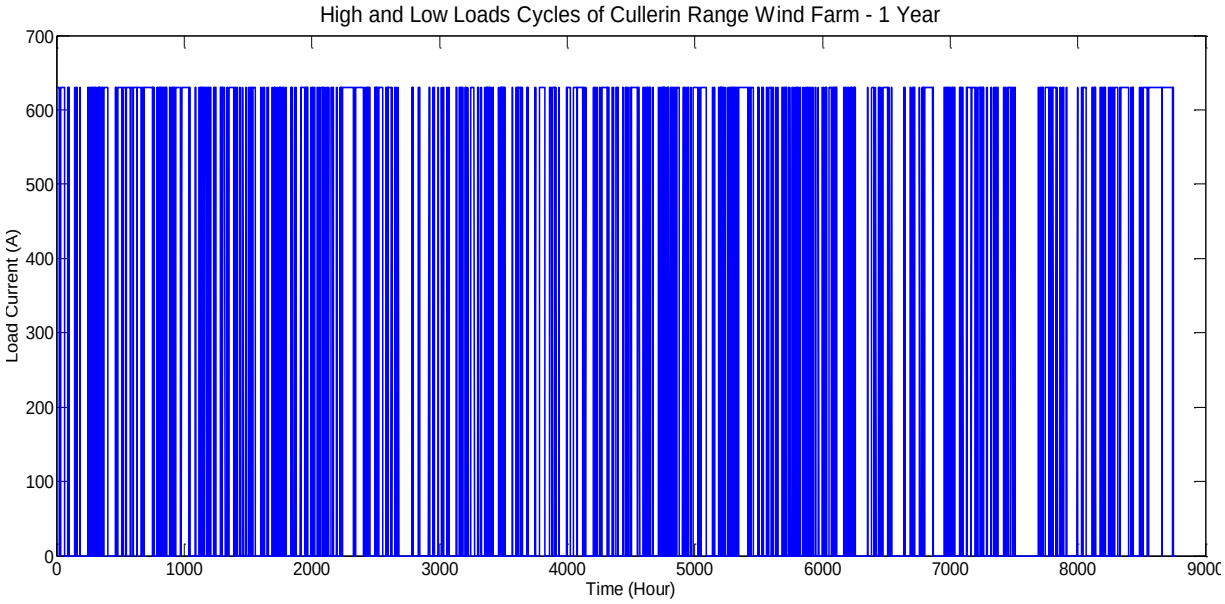

Figure 5.7: Time Distribution for Fitted High and Low Loads

Figure 5.7 shows how these high and low loads are distributed against time over the year which are then used to produce the PDF of high load cycle widths shown in Figure 5.8 where the loads are grouped in 6 hour intervals.

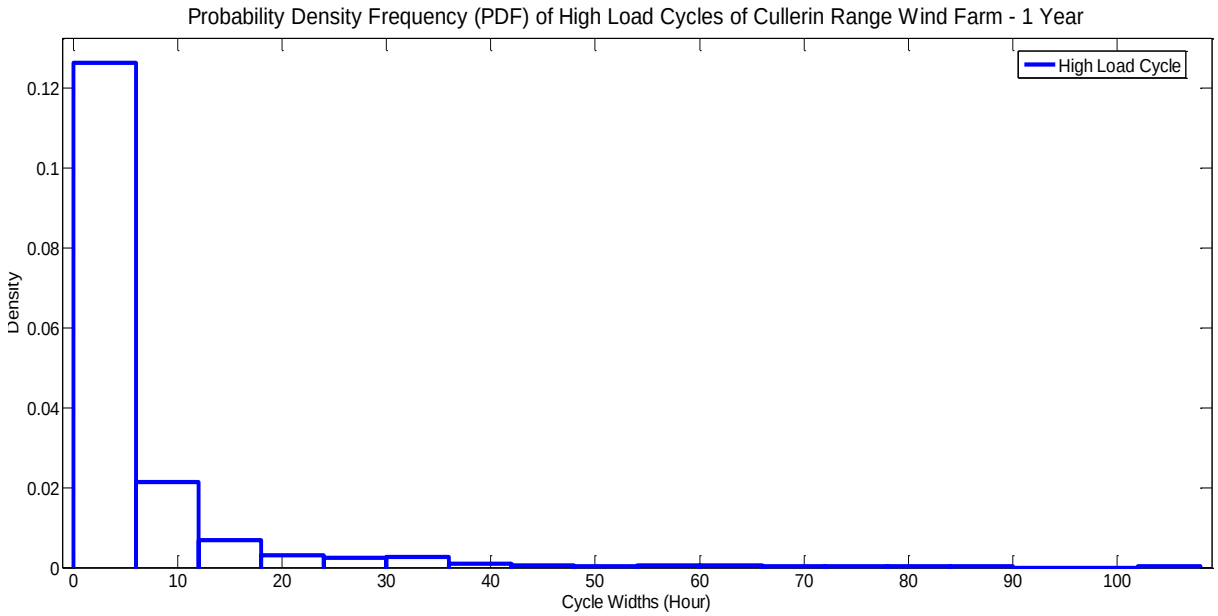

Figure 5.8: PDF of High Load Cycles Width of Cullerin Range Wind Farm for 1 Year

From the PDF plot, it is observed that the shortest cycle width of 0-6 hours occurred most frequently with PDF of 0.756 (approx. 75% of the time). In terms of frequency, the next most common time durations are cycle loads of 6-12 hours at 0.127 (approx. 13% of the time), 12-18 hours at 0.0409 (4%) and 18-24 hours 0.0189 (1.9%). Therefore cycles of 24 hours or less make up almost 94% or all cycle durations with cycles of 48 hours or less increasing that to 97.9%. The probability of the longest load cycle widths of 108 hour are only 0.15%. Given the long thermal time constant seen at the landfall, it is clear that the cable would not attain a full steady state temperature rise.

The most important observation is that the high majority of high load cycles are only for sustained periods of less than 2 days (98% of the time). This supports the cyclic models created in Chapter 4 which test 4 variations of cycle with length of under 48 hours.

Figure 5.9 shows a PDF of the low load cycle widths also grouped in 6 hour intervals from 0-180 hours.

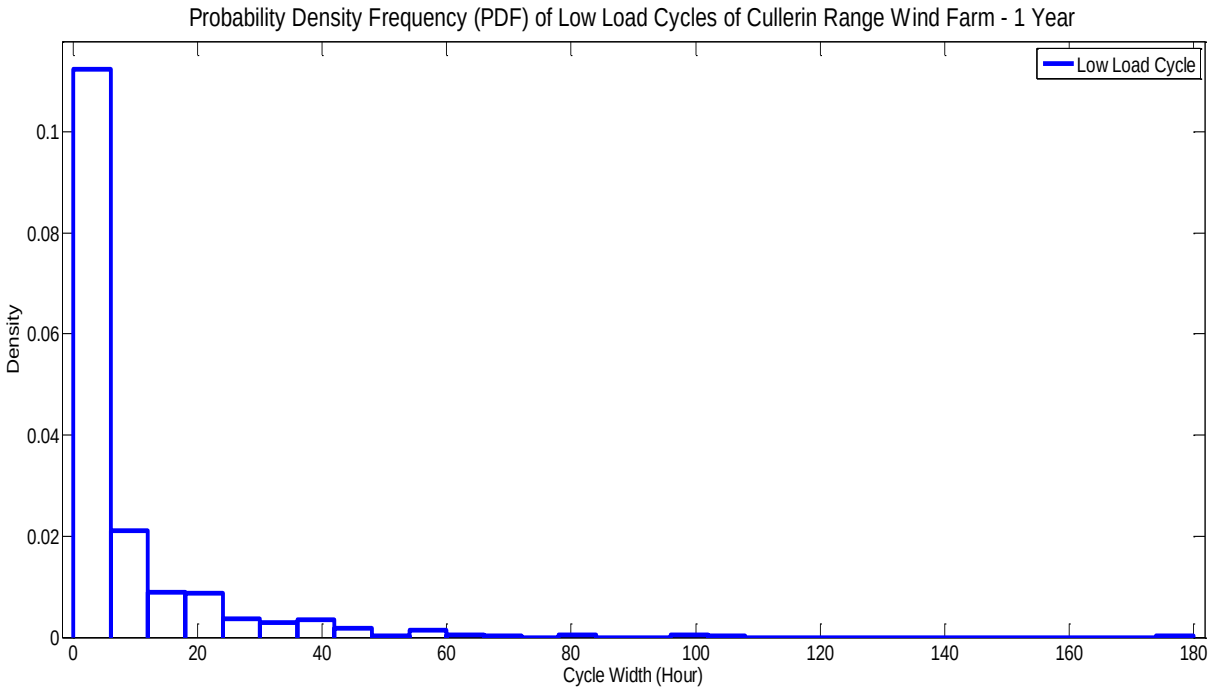

Figure 5.9: PDF of Low Load Cycles Width of Cullerin Range Wind Farm for 1 Year

It is observed that the shortest cycle width of 0-6 hours occurred most frequently with PDF of 0.6738 which is approximately 67% of the time. The next most common time durations are cycle loads of 6-12 hours at 0.126 (approx. 13% of the time), 12-18 hours at 0.0535 (5%) and 18-24 hours 0.0519 (5%). Cycles of 24 hours or less make up almost 88% or all cycle durations with cycles of 48 hours or less increasing that to 97.6%.

The probability of the longest load cycle widths of 180 hour is only 0.15%. It is observed that the longest sustained low load cycle duration is considerably longer than the longest high load duration, however it should be considered that any service outage would show in low load data, and while the data can't distinguish what duration may be caused by outage, some percentage of downtime during the 1 year period should be assume. Outage for maintenance (rather than due to cut out from extreme environmental conditions) may be responsible for the longer periods.

This also suggests that the duration of low load cycles are typically only sustained for less than 2 days (98% of the time). This also supports the cyclic durations of 48 hours and less modelled in Chapter 4.

Comparing PDF plots, there are some observations that can be deduced for the behaviour for high and low load cycle widths. Both loads have no prolonged periods of cycle widths. The sustained cycle periods for both are typically less than 2 days. Both loads have the highest PDF for cycle period of less than 6 hours which average 71% of the time. These short duration cycle trends also show that the highly volatile loads generated by wind farms are suitable for a cyclic rating approach, since the periods of the cyclic load increase 'on time' are much shorter than the thermal time constant; a difference that will show a more significant increase in rating is attainable.

5.4 Identification of Exceedance

This section compares cable temperature obtained from Cullerin Range Wind Farm data with the 5 different cyclic loads simulated in Chapter 4 and identifies the probability that the Cullerin Range wind data peak Tc will exceed the peak Tc of each simulated cyclic load.

This provides an indication of the risk level associated with using each cyclic load, as a basis for calculating a more accurate cable rating. A load with a risk level of zero represents a risk free base on which an increased cable rating could be further investigated, by increasing load within the cable thermal limitations. Conversely, a cyclic load with a risk level above zero, indicates that the wind farm output would exceed the Tc of the load profile. The higher the risk level, the higher the probability of Tc exceedance and the lower the suitability.

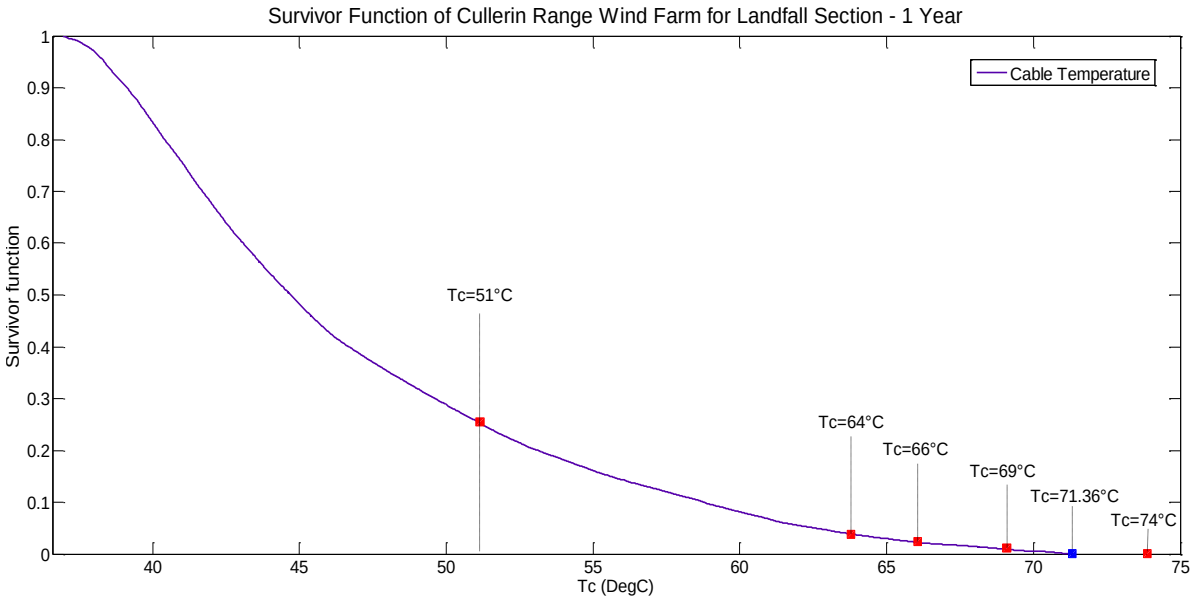

Figure 5.10: Survivor Function of Cable Temperature of Cullerin Range Wind Farm for Landfall Section for 1 Year

Figure 5.10 shows the probability of the Cullerin Range wind farm peak conductor temperature (Tc = 71.36°C) exceeding the peak Tc of each cyclic load profile. Table 5.1 shows these results with the probability shown as a % Risk Factor that the wind farm Tc will exceed that of the cyclic loads Tc.

Table 5.1: Comparison of Cable Temperatures

Cyclic Models (cycle durations)		**Cullerin Range Peak Tc (630A)**	**Cyclic Model Peak Tc (630A)**	**Comparison of Cullerin Range Peak Tc with each Cyclic Model Peak Tc**	
High Load	Low Load	Temp°C	Temp°C	Exceedance	% Risk Factor
6 hour	18 hour	71.36	51	Yes	25.68%
12 hour	12 hour	71.36	64	Yes	3.7%
18 hour	6 hour	71.36	74	No	0%
24 hour	24 hour	71.36	66	Yes	2.23%
48 hour	48 hour	71.36	69	Yes	0.96%

It is observed that the highest risk factor of 25.68% is seen from the 6 hour high and 18 hour low load cycle. With such a short high load and long low load, the peak Tc only reaches 51°C. A revised cable rating based on this cyclic load would be unrealistically high, making this load cycle (and any rating obtained from it) unsuitable for the design of the cable system.

The trend observed from the wind farm data, that sustained load duration rarely exceeds 2 days, which means the 48 hour high and low load cycle has a low risk probability of only 0.96%. This indicates that this cyclic pattern has more than 99% reliability of not exceeding the Cullerin Range data, however this still represents a risk that cannot be overlooked.

The lowest exceedance is from the 18 hour high and 6 hour low load pattern, indicating 0% risk for this cyclic load.

To further analyse the 18 hour high and 6 hour low load cycle, the normalised Cullerin Range wind data is re-scaled using the cyclic rating (725A) obtained for this load cycle in Chapter 4. The simulated Tc results (Year 4) obtained are shown in Figure 5.11.

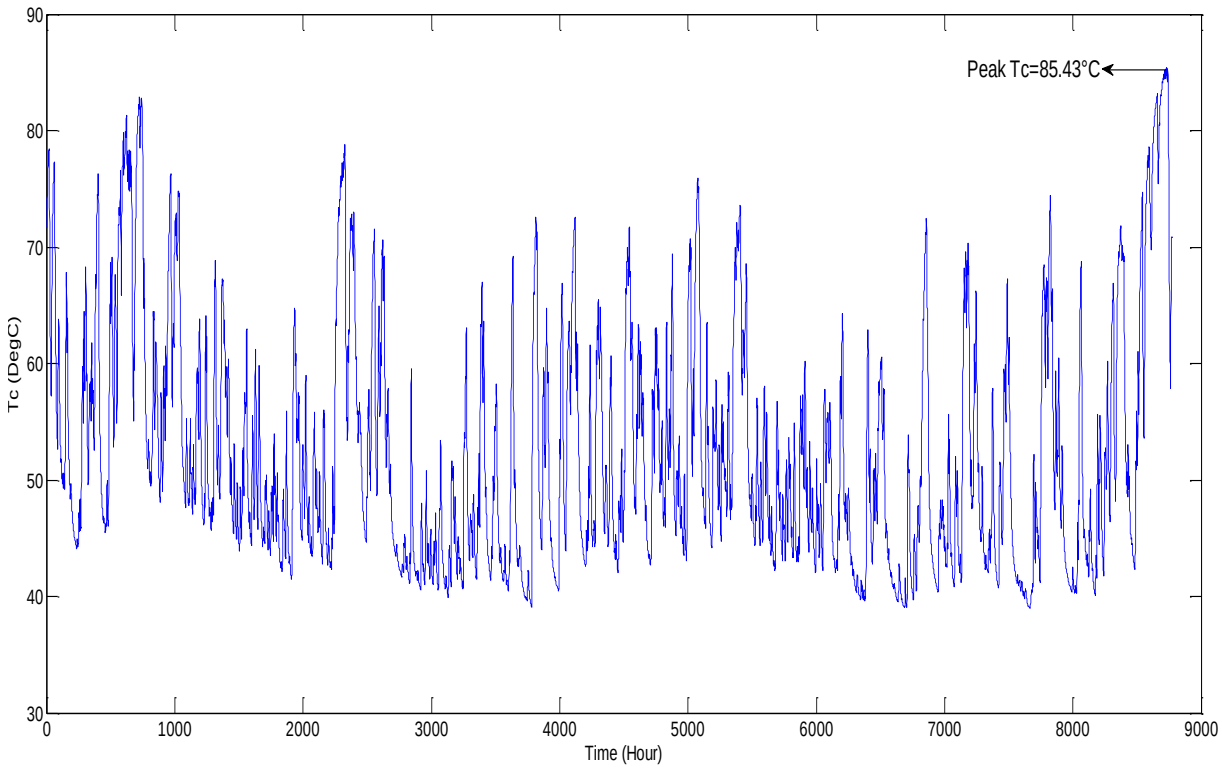

Figure 5.11: Cable Temperature of Cullerin Range Wind Farm Normalised with 725A (Cyclic Rating) for Landfall Section for 1 Year

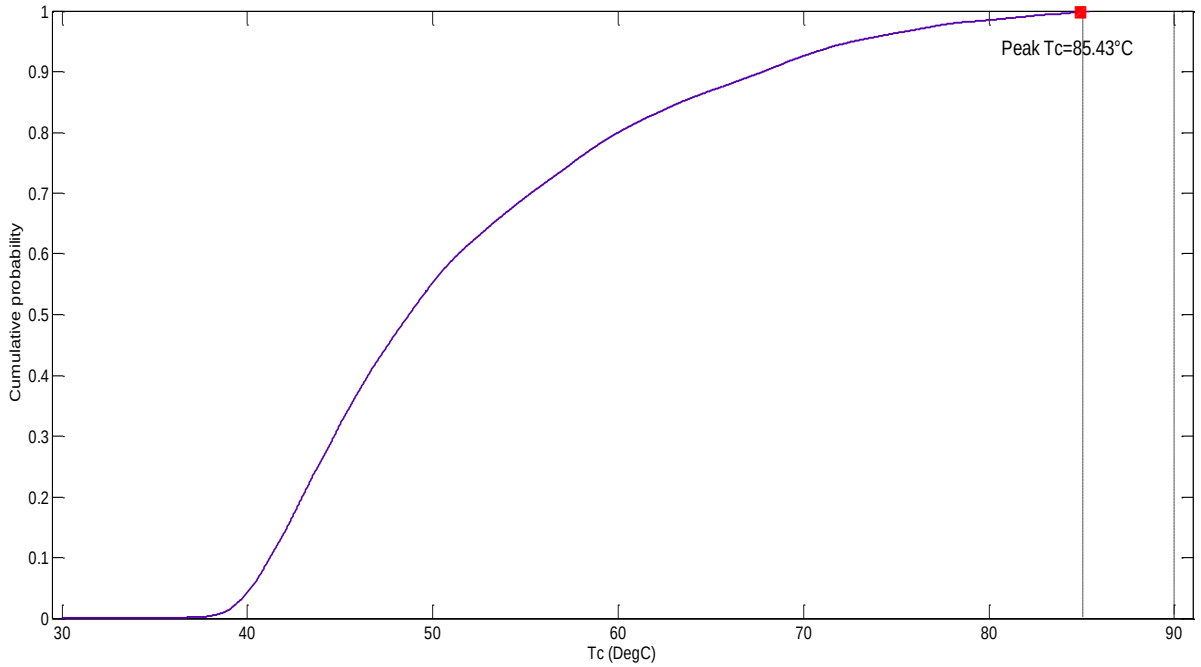

Figure 5.12: Cumulative Probability Distribution (CDF) of Cable Temperature of Cullerin Range Wind Farm Normalised with 725A (Cyclic Rating) for Landfall Section for 1 Year

A peak Tc of 85.43°C is observed, 4.57°C below the cable limit of 90°C, equivalent to a tolerance of 5.07%.

This result supports the increased cable rating of 725A proposed in Chapter 4 with tolerances observed in two places (within the exceedance of the load pattern where 0% risk of exceedance at 630A showed a Tc tolerance of 2.64°C above the Cullerin Range Tc of 71.36°C, and at the increased load where Tc peaks at 4.57°C below cable limit).

Therefore, based on comparisons to the Cullerin Range wind farm data, there is no evidence that cable limits will be exceeded when cyclically rating the cable at 725A, equating to an increase of 15.07% over the standard steady state rating of 630A.

5.5 Summary

This chapter utilised normalised wind power data from Cullerin Range wind farm to analyse the risk of exceedance for the design of the cable system using cyclic methodology. One year of Cullerin Range wind farm power data is applied to the landfall FEA model set in summer ambient temperature of 30°C and buried at 3m in depth. Load currents are classified into high and low loads to obtain the PDF of high and low load cycle widths. The purpose is to establish any trends present in the wind farm data that can be compared to the 5 cyclic loads simulated in Chapter 4.

Comparison are then used to assess the risk of cable temperature exceedance for these 5 different cyclic load patterns, to see which will be the most suitable base case for an increased cable rating.

Results showed that a cyclic load of 18 hour high and 6 hour low load gives 0% risk of exceeding the Tc of the Cullerin Range data at the steady state rated load of 630A. Increasing the Cullerin Range data load to the rating obtained from the cyclic load in Chapter 4 (725A) resulted in a peak temperature of 85.43°C, safely within cable temperature limit.

Chapter 6

Conclusion and Future Work

This chapter concludes the work done and results obtained from the whole research. Possible recommendations are suggested to carry on for future research.

6.1 Conclusion

This research work on HVAC cable rating techniques explores a variety of methods for obtaining a more accurate cable rating using non-steady-state technique. Researchers have shown that the use of FEA, cyclic and probabilistic rating techniques offer a strong indication that rating accuracy can be improved, compared to the traditional steady state methods used to rate wind farm export cables.

This report utilised a three-core HVAC 132kV XLPE cable model built in commercial FEA software Comsol. Once built, the model was then analysed and simplified by way of optimising time stepping in the model, followed by sensitivity analysis to establish which elements of the cable could be merged together without compromising the accuracy of the model. Time steps of 300, 600, 1800 and 3600 seconds were tested to find a suitable duration that would save computational time without compromising accuracy. A time step of 1800 seconds was deemed most suitable and used for all models. The result of the sensitivity analysis saw individual armour wires merged into a single domain; the conductor screen, dielectric screen and water tape merged with the conductor, and the binder tape and fillers removed completely. Using these methods to simplify the model resulted in a significant reduction of computational time. The fully detailed model for a 48 hour transient state took approximately 20 minutes to solve. The sensitivity analysis reduced this to 4 minutes.

Three cable sections (buried at sea, landfall and J-tube in air sections) run from the land based substation to the offshore windfarm and a model of each section was built for thermal analysis. The cyclic rating of a cable is based on a load that is repeated cyclically, so a set of 5 cyclic load profiles (3 daily, one 48 hour and one 96 hour) were run for each cable model. All cycles

used a flat top load cycle with a high load of 630A (the cable steady state rating) and a low load of 0A (zero amps). Ambient conditions were based on peak summer temperatures based on data obtained from the National Grid and the Met Office. Results showed significant potential for increasing the rating for the buried at landfall and subsea sections.

One year of normalised wind farm data obtained from the Cullerin Range Wind Farm was used as a comparison to analyse the risk of Tc exceedance for each of the cyclic load profiles, based on the landfall cable section. Data was classified into high and low loads and distributed against time over the year, and then used to produce a PDF of high/low load cycle widths that could be analysed for trends. Over 97% of cycles observed were below 48 hours. With durations similar to the cyclic load profiles, comparisons were made to find which profile showed least risk of Tc exceedance, therefore being the safest option for increased cable rating.

Designing a cable system using cyclic rating obtained from the 18 hour high and 6 hour low load cycle, showed 0% risk of exceeding the cable system limits and a potential to increase the cable rating from 630A to 725A equivalent to a 15% underutilisation. The Cullerin Range data load was increased to 725A with results showing a peak temperature reached is only 85.43°C, safely within cable temperature limit. Although only one set of actual wind farm data has been used in estimating potential exceedance for each cycle, it still shows promising results for the use of cyclic rating methodology, with sizeable level of underutilisation of the standard steady state rating technique.

6.2 Recommendations for Future Work

Although the work presented in this report shows positive results for non-steady state cyclic rating methodology, there are a number of way it can be further improved.

1) Load datasets from more actual wind farms can be used for comparison of cable temperature exceedance to support the reliability of using cyclic methods. A study of datasets based on different parts of United Kingdom may reveal trends across the region. Future planning for offshore wind farms can use the collected trends as a baseline.

2) Create FEA models focussing on the cable joints as these sections are known as another major hot spot in the cable route, and use revised cable ratings from this study to investigate potential issues.
3) The fluctuations in power generated by a wind farm, environmental thermal parameters such as ambient temperature, soil/sand resistivity and solar radiation, are subject to random variations. Probability distributions of these parameters could be determined and added to create a probabilistic rating method. This could integrate scientific predictions on the long term effect of global warming on the cable environment (sea, soil temperatures rising) over the estimated lifespan of a cable.
4) Several years of windfarm load data can be used to obtain correlation trends and a probability density plot can be used to look for month on month trends across all years, as well as any instances of irregular behaviour. The seasonal trends will be expected to be seen but irregular behaviour is unlikely due to extreme weather events being generally short lived and there being a shut off for wind farms in the event of extreme weather.
5) Due to the short thermal time constant for J-tube in air section, probabilistic methods can be tested on this section incorporating air ambient and solar radiation, which have huge variations from summer to winter seasons.
6) The unpredictable nature of output power from wind farms, using different statistical methods to forecast and 'smoothen' wind power fluctuations based on different time scales to create a flat-topped cycle that can be use in cyclic rating methodology.
7) Create a synthetic wind farm dataset to justify the rating method by preserving correlation to, and randomness of, the historical wind power data. The historic wind power data can be used to create future synthetic test data for the model by using auto-regression [76] to create a forecast model from which error values can be obtained (the difference between the actual data and the forecast data). Standard deviations can be obtained from these errors and used to create more random data within the boundaries set by them. Wind data is always random, so this method is intended to maintain that randomness as well as a correlation to the original data.

Bibliography

[1] EEA, Europe's onshore and offshore wind energy potential. EEA Technical Report. European Environment Agency, 2009.

[2] A. R. Henderson, C. Morgan, B. Smith, H. C. Sorensen, R. J. Barthelmie, and B. Boesmans. Offshore Wind Energy in Europe? A Review of the State-of-the-Art, Wind Energy, 6:35-52, 2003.

[3] E.ON. E.ON Wind Turbine Technology and Operations Fact book. September 2013.

[4] IEC. Electric Cables - Calculation of current rating - Part 1-1: Current rating equations (100% load factor) and calculation of losses - general. Technical report, IEC 287-1-1. International Eletroctechnical Commission, 2006.

[5] T. Obdam, H. Braam, R. V. De Pieterman, and L. Rademakers. O&M Cost Estimation & Feedback of Operational Data, 2011.

[6] European Wind Energy Association (EWEA). Wind Energy - The Facts, Brussels, European Wind Energy Association. March 2009. Available: http://ewea.org. Accessed March 2014

[7] R. Green and N. Vasilakos. The Economics of Offshore Wind, Energy Policy, 39:496-502, February 2009.

[8] EIA. Hong Kong Government - Offshore Wind Farm Project, 2006.

[9] T. Worzyk. *Submarine Power Cables - Design Installation Repair Environment Aspects.* Springer, 2009

[10] A. R. A. Raja, B. Vissouvanadin, T. T. N. Vu, G. Teyssedre, and N. I. Sinisuka. Space Charge Measurement on XLPE Cable for HVDC Transmission using PEA Method, *Procedia Technology*, 11: 327-333, 2013.

[11] W. Choo and G. Chen. Electric Field Determination in DC Polymeric Power Cable in the Presence of Space Charge and Temperature Gradient under DC conditions, *International Conference on Conditioning Monitoring and Diagnosis*, pp. 321-324, Beijing, China, 21-24 April 2008.

[12] C. Savvidou. Centrifuge modelling of heat transfer in soil. *Centrifruge 88,* Rotterdam, 1988.

[13] G.J. Anders. *Rating of Electric Power Cable:* A*mpacity Computations for Transmission, Distribution, And Industrial Applications*. Institute of Electrical & Electronics Engineers (IEEE) McGraw Hill, 1st January 1997.

[14] IEC. Electric Cables - Calculation of the Current Rating - Part 2: Thermal Resistance - Section 2.1. Calculation of thermal resistance. Technical Report, *International Electrotechnical Commissi*on., 1994.

[15] G.F. Moore. *Electric Cables Handbook-BICC Cables.* Blackwell Science Ltd, 3rd Edition, 1997.

[16] N. Idir, Y. Weens, and J-J .Franchaud. Skin effect and Dielectric Loss Models of Power Cables. *.IEEE Transactions on Dielectric and Electrical Insulation,* 16(1):147-154, February 2009.

[17] A.O.E. Gouda and A. A. Farag. Factors Affecting the Sheath Losses in Single-Core Underground Power Cables with Two-Points Bonding Method, *International Journal of Electrical and Computer Engineering (IJECE),* 2:7-16, February 2012.

[18] D. Palmgren. Armour Loss in three-core submarine XLPE cables-ABB High Voltage cables, 23rd April 2013.

[19] M. Coates. *ERA rating in J-tube,* ERA Technology Ltd 88-0108, March 1988.

[20] J.J. Bremnes, G. Evenset, and R. Stolan. Power loss and inductance of steel armoured multi-core cables-comparison of IEC values with 2.5D FEA results and measurements - B1_116_2010, presented at the *Cigre* Paris, France, 2010.

[21] D. Palmgren, J. Karlstrand, and G. Henning. Armour Loss in Three-Core Submarine XLPE Cables, presented at the *8th International Conference on Insulated Power Cables-Jicable'11,* Versailles- France, 2011.

[22] University of Southampton, EPE Virtual Learning Course - Cables, 2012.

[23] H.J. Joergensen, J. Hjerrild, C. Jensen, and J. Havsager. Improved Operation of cables connecting offshore wind farms to the power grid, presented at the *Cigre* Paris, France, 2004.

[24] J.H. Neher and M.H. McGrath. The Calculation of the Temperature Rise and Load Capacity of Cable Systems. *IEE Transactions on Power Apparatus and Systems,* Part III, 1957.

[25] T.R. Blackburn, University of New South Wales - Equipment Rating.

[26] D.J. Swaffield, P.L. Lewin, and S.J. Sutton. The use of finite element analysis modelling to improve the precision of high voltage cable ratings. 1*0th INSULCON International Electrical Insulation Conference,* pp.155-161, Birmingham, UK, 2006.

[27] D. J. Swaffield, P. L. Lewin, and S. J. Sutton. Methods for rating directly buried high voltage cable circuits, *IET Generation, Transmission & Distribution,* 2(3):393-401, 2008.

[28] M.S. Baazzim, M.S. Al-Saud, and M.A. El-Kady. Comparison of Finite-Element and IEC Methods for Cable Thermal Analysis under Various Operating Environments, *International Journal of Electrical, Robotics, Electronics and Communications Engineering,* 8:476-481, 2014.

[29] M. Stonjanovic, D. Tasic, and A. Ristic. Cyclic Current Ratings of Single-Core XLPE Cables with Respect to Designed Life Time, 89(5):152-156, Prezeglad Elektrotechniczny, 2013.

[30] J. Schachner. Power connection for Offshore Wind Farms, University of Leoben, Austria 2005.

[31] J.J. Desmet, D.J. Putman, G.M. Vanalme, and R.J. Belmans. Modelling and Sensitivity Analysis of the Thermal behaviour of cables for different current conditions. *11th IEEE*

International Conference on Harmonics and Quality of Power, pp 471-476, 12-15 September 2004.

[32] X. Yuan, H.P. Fleischer, G. Sande, and L.J. Solheim. Integration of IEC 60287 in Power System Load Flow for Variable Frequency and Long Cable Applications, *International Journal of Electrical Energy*, 1(1):6-11, March 2013.

[33] R. Mardiana. Parameters Affecting the Ampacity of HVDC Submarine Power Cables. *2nd International Conference on Power, Energy & Industry Applications,* pp 1-6, 15-17 November 2011.

[34] IEC. Calculation of the cyclic and emergency current rating of cables: Part 2: Cyclic rating of cables greater than 18/30 (36) kV and emergency ratings for cables of all voltages. Technical report, International Electrotechnical Commission, 1989.

[35] G.P. Nikishkov. *Introduction to the Finite Element Method*, University of Aizu, Japan 2004.

[36] N. Flatabo. Transient Heat Conduction Problems in Power Cables solved by Finite Element Method. *IEEE Transactions on Power Apparatus and Systems*, 92(1):56-63, January 1973.

[37] M.S. Al-Saud, M.A. El-Kady, and R.D. Findlay. Accurate Assessment of Thermal Field and Ampacity of Underground Power Cables. *Canadian Conference on Electrical and Computer Engineering, CCECE '06,* pp 651-654, Ottawa, Canada, May 2006.

[38] F. d. Leon and G.J. Anders. Effect of Backfilling on Cable Ampacity Analyzed with the Finite Element Method. *IEEE Transactions on Power Delivery*, 23(2):537-543, April 2008.

[39] J. A. Pilgrim, D. J. Swaffield, Paul.L. Lewin, S. T. Larsen, F. Waite, and D. Payne. Rating Independent Cable Circuits in Forced-Ventilated Cable Tunnels. *IEEE Transaction on Power Delivery*, 25(4):2046-2053, 2010.

[40] D. J. Swaffield, P. L. Lewin, S. T. Larsen, and D. Payne. Effects of modelling assumptions on the rating calculation for externally forced cooled high-voltage cables. *IET Generation, Transmission & Distribution*, 3(5): 496-507, 2009.

[41] J. A. Pilgrim, D. J. Swaffied, P. L. Lewin, S. T. Larsen, and D. Payne. Assessment of the Impact of Joint Bays on the Ampacity of High-Voltage Cable Circuits. *IEEE Transactions on Power Delivery*, 24(3):1029-1036, July 2009.

[42] S. Kahourzade, A. Mahmoudi, B. N. Taj, and O. Palizban. Ampacity Calculation of the Underground Power Cables in Voluntary Conditions by Finite Element Method. *8th Electrical Engineering/Electronics, Computer, Telecommunications and Information Technology (ECTI) Association of Thailand*, Thailand, 2011.

[43] G. Idicula and A.E. Davis. The Probabilistic Rating of Separate-cooled Cables. *IET 3rd International Conference on Probabilsitic Methods Applied to Electric Power Systems*, pp 185-190, London, 3-5 July 1991.

[44] G. Idicula. The Probabilistic Rating pf Separate-cooled Cables, Doctorate of Philosophy, School of Electronic and Conputer Science, University of Southampton, 1990.

[45] C.F .Proce and R.R. Gibbon. Statistical approach to thermal rating of overhead lines for power transmission and distribution, *IEE Proceedings Generation, Transmission and Distribution*, 1983.

[46] B.M. Weedy. *Thermal Design of Underground Systems*. Southampton: John Wiley & Sons, 1988.

[47] A.K. Blackwell, A.E. Davis, C. Ong-Hall, and S.T. Larsen. Forecasting Cable Ratings using a probabilistic Method and Real Time Parameter Values. *Sixth International Conference on AC and DC Power Transmission*, (423):81-85, 29th April-3rd May 1996.

[48] A.K. Blackwell. Forecasting and Probabilistic Rating of Underground Power Cables Doctorate of Philosophy School of Electronic and Conputer Science, University of Southampton, 1996.

[49] M.A. El-Kadt, F.Y. Chu, H. Radhakrishna, D.J. Horrocks, and R. Ganton. A Probabilistic Approach to Power Cable Thermal Analysis and Ampacity Calculation. *IEEE Power Engineering Review*, PAS-103(9): 2735-2740, September 1984.

[50] S.M. Forty, G.J. Anders, and S.J. Croall. Cable environment analysis and the probabilistic approach to cable rating. *IEEE Transaction on Power Delivery*, 5(3):1628-1633, July 1990.

[51] H.C. Zhao, J.S. Lyall, and G. Nourbakhsh. Probabilistic Cable Rating Based on Cable Thermal Environment Studying. *International Conference on Power System Technology Proceedings, Power Con*, 2:2071-1076, December 2000.

[52] J.E. Steinmanes. Thermal property of measurements using a thermal probe. *Proceedings of the symposium on underground cable thermal backfill*, Toronto. Canada, 1981.

[53] Cigré. Computer method for the calculation of the response of single-core cables to a step functional thermal transient, *Electra*, 87, 1983.

[54] P.L. Stephenson. The use of superposition for transient ratings of naturally and forced cooled buried cables. CEGB unrestricted research report no.TPRDL/L/3288/R88, 1988.

[55] J.S. Lyall. Cable on-line monitoring analysis. *Australian Power Technologies Transmission & Distribution*, 2012.

[56] A.M. Costa, G. Roshan, J.A. Orosa, and A. Rodriguez-Fernandez. Case study of Weather Maintenance in Wind Power Generation, *Earth Sciences*, 39:5615-5624, 22 April 2014.

[57] W. Zhang, C.D. Markfort, and F. Porte-Agel. Experimental Study of the impact of large-scale wind farms on land-atmosphere exchanges, *IOPScience*, 8:1-8, 2012.

[58] B. Vahidi and A. Mahmoudi. Determination of the Ampacity of Buried Cable in Non-Homogenous Environmental Condition by 3D Computation, *Journal of Electrical Engineering & Technology*, 7(3):384-388, 2012.

[59] Cullerin Range Wind Farm. Available: http://www.windfarmperformance.info/. Accessed December 2013

[60] National Grid and Neta Elexon Electric : BM Reports - Generation by Fuel Type. Available: http://www.bmreports.com/bsp/bsp_home.htm. Accessed December 2012

[61] S. Park, C. Deser, and M.A. Alexander. Estimation of the Surface Heat Flux Response to Sea Surface Temperature Anomalies over the Global Oceans, *Journal of climate*, 18(21):4582-4599, 1 November 2005.

[62] J. A. Pilgrim, S. Catmull, R. Chippendale, P. L. Lewin, P. Stratford, and R. Tyreman. Current Rating Optimisation for Offshore Wind Farm Export Cables, *Cigré*, France, Paris, 2014.

[63] P.J.S. Statoil. J-tube and scour protection - Sheringham Shoal Offshore Wind Farm. June 2011.

[64] M.B. Zaaijer. Comparison of monopile, tripod, suction bucket and gravity base design for a 6MW turbine. *Offhsore Wind and Other Marine Renewable Energies in Mediterranean and European Seas (OWEMES)*, 2003.

[65] ISO 13628-5: Petroleum and natural gas industrial - Design and operation of subsea production systems - Part 5: Subsea Umbilicals, 2009.

[66] R.A. Hartlein and W.Z. Black. Ampacity of Electric Power Cables in Vertical Protective Risers. *IEEE transaction on power apparatus and systems*, PAS-102(6):1678-1682, June 1983.

[67] H.Y. Wong, *Heat Transfer for Engineers*. London: Longman Group United Kingkom, 1977.

[68] J.A. Pilgrim, D.J. Swaffield, P.L. Lewin, S.T. Larsen, and D. Payne. Use of Finite Element Analysis to Obtain Thermal Ratings for High Voltage Cable Joint Bays. *EIC-IEEE Electrical Insulation Conference*, Montreal, QC, Canada, pp 224-227, 31st May-3rd June 2009.

[69] P.L. Lewin, J.E. Theed, A.E. Davis, and S.T. Larsen. Methods for rating power cables buried in surface troughs. *IEEE Proceedings of Generation, Transmission and Distribution*, 146(4):360-364, July 1999.

[70] K.-Y. Lee, J.-S. Yang, Y.-S. Choi, and D.-H. Park. Specific Heat and Thermal Conductivity Measurement of XLPE Insulator and Semiconducting Materials. *IEEE 8th International Conference on Properties and Applications of Dielectric Materials*, pp 805-809, Bali, Indonesia, June 2006.

[71] C. A. Long. *Essential Heat Transfer*. Pearson Education Limited, Harlow, England, 1st edition, 1999.

[72] H. R. Skjoldal. Update report on North Sea Conditions - 2nd quarter 2007, 2007.

[73] R. Chippendale, P. Cangy, J. Pilgrim. Thermal Rating of J tubes using Finite Element Analysis Techniques. *Jicable 9th International Conference on Insulated Power Cables*, Versailles, France, 21st -25th June 2015.

[74] Technical Specifications TS 2.05, National Grid 2010.

[75] Cigré. Current Ratings of Cables for Cyclic and Emergency Loads, *Electra*, 24, 1964.

[76] P. Gomes and R. Castro. Wind Speed and Wind Power Forecasting using Statistical Models: AutoRegressive Moving Average (ARMA) and Artificial Neural Networks (ANN). *International Journal of Sustainable Energy Development (IJSED),* 1(1/2):36-45, March/June 2012.